OPEN ACCESS
CellPress

Cell Reports
Article

Targeting Polycomb to Pericentric Heterochromatin in Embryonic Stem Cells Reveals a Role for H2AK119u1 in PRC2 Recruitment

Sarah Cooper,[1] Martin Dienstbier,[2] Raihann Hassan,[1] Lothar Schermelleh,[3] Jafar Sharif,[4] Neil P. Blackledge,[5] Valeria De Marco,[6] Sarah Elderkin,[7] Haruhiko Koseki,[4] Robert Klose,[5] Andreas Heger,[2] and Neil Brockdorff[1,*]
[1]Developmental Epigenetics, Department of Biochemistry, University of Oxford, Oxford OX1 3QU, UK
[2]CGAT, MRC Functional Genomics Unit, Department of Physiology, Anatomy and Genetics, University of Oxford, Oxford OX1 3PT, UK
[3]Advanced Cellular Imaging, Department of Biochemistry, University of Oxford, Oxford OX1 3QU, UK
[4]Laboratory for Developmental Genetics, RIKEN Center for Integrative Medical Sciences, 1-7-22 Suehiro, Tsurumi-ku, Yokohama 230-0045, Japan
[5]Chromatin Biology and Transcription, Department of Biochemistry, University of Oxford, Oxford OX1 3QU, UK
[6]MRC National Institute for Medical Research, The Ridgeway, Mill Hill, London NW7 1AA, UK
[7]Nuclear Dynamics, Babraham Institute, Babraham Research Campus, Cambridge CB22 3AT, UK
*Correspondence: neil.brockdorff@bioch.ox.ac.uk
http://dx.doi.org/10.1016/j.celrep.2014.04.012

SUMMARY

The mechanisms by which the major Polycomb group (PcG) complexes PRC1 and PRC2 are recruited to target sites in vertebrate cells are not well understood. Building on recent studies that determined a reciprocal relationship between DNA methylation and Polycomb activity, we demonstrate that, in methylation-deficient embryonic stem cells (ESCs), CpG density combined with antagonistic effects of H3K9me3 and H3K36me3 redirects PcG complexes to pericentric heterochromatin and gene-rich domains. Surprisingly, we find that PRC1-linked H2A monoubiquitylation is sufficient to recruit PRC2 to chromatin in vivo, suggesting a mechanism through which recognition of unmethylated CpG determines the localization of both PRC1 and PRC2 at canonical and atypical target sites. We discuss our data in light of emerging evidence suggesting that PcG recruitment is a default state at licensed chromatin sites, mediated by interplay between CpG hypomethylation and counteracting H3 tail modifications.

INTRODUCTION

Polycomb group (PcG) repressor proteins play an important role in developmental gene regulation in multicellular organisms (Ringrose and Paro, 2004). In most cases, they are assigned as components of one of two major multisubunit complexes, Polycomb repressive complex 1 (PRC1) and PRC2, both of which have intrinsic histone-modifying activities (monoubiquitylation of histone H2A lysine 119 [H2AK119u1] and methylation of histone H3 lysine 27 [H3K27me1/2/3], respectively; reviewed in Simon and Kingston, 2013). Vertebrates possess several variant PRC1 complexes, as defined by the presence of the subunit PCGF1-6 (Gao et al., 2012). The histone-modifying activities of PRC1 and PRC2 are of central importance for PcG function (Endoh et al., 2012; Pengelly et al., 2013), although several studies have revealed that PRC1 also mediates repression through alternative mechanisms (Eskeland et al., 2010; Francis et al., 2004; Isono et al., 2013). Canonical PRC1 and PRC2 function in a hierarchical manner, with PRC1 recruitment occurring via binding of the chromodomain of the Cbx Polycomb subunit to PRC2-mediated H3K27me3 (Cao et al., 2002; Wang et al., 2004). More recent studies have demonstrated that variant PRC1 complexes are recruited through PRC2-independent mechanisms (Schoeftner et al., 2006; Tavares et al., 2012).

In vertebrates, cytosine residues at CpG dinucleotides are extensively methylated, with the exception of CpG islands (CGIs), which are found at the promoter region of more than 50% of genes (reviewed in Illingworth and Bird, 2009). DNA methylation is required for normal development, but not for the maintenance of embryonic stem cells (ESCs) in vitro (reviewed in Bestor, 2000). DNA methylation patterns are erased in early embryos and developing germ cells, and are then reestablished by the de novo DNA methyltransferases Dnmt3a and Dnmt3b, and the accessory protein Dnmt3L (reviewed in Reik et al., 2001). Propagation of DNA methylation patterns through DNA replication is dependent on the maintenance DNA methyltransferase, Dnmt1, and the accessory protein Uhrf1 (Bestor, 2000; Sharif et al., 2007).

In *Drosophila*, PcG recruitment at Hox loci, as well as other targets, is mediated by transcription factor binding at sequences designated as Polycomb response elements (Kassis and Brown, 2013; Mohd-Sarip et al., 2005). In mammalian cells, PcG proteins are recruited to target gene promoters and also to atypical sites, specifically the inactive X chromosome (de Napoles et al., 2004; Plath et al., 2003; Silva et al., 2003), and paternal pericentric heterochromatin (PCH) domains in early mouse embryos (Puschendorf et al., 2008; Santos et al., 2005). There is evidence

supporting a role for sequence-specific factors in PcG recruitment in mammals (Woo et al., 2010, 2013), and also suggesting a role for noncoding RNA (reviewed in Brockdorff, 2013). Additionally, several studies have demonstrated a link between unmethylated CpG residues and PcG recruitment/binding. Specifically, PcG occupancy correlates closely with CpG density in CGIs at target gene promoters (Lynch et al., 2012; Mendenhall et al., 2010). Moreover, depletion of DNA methylation has been correlated with changes in patterns of PRC2 localization (Brinkman et al., 2012; Reddington et al., 2013). Linked to these observations, recent studies have demonstrated that recruitment of the variant PRC1 complex PCGF1-PRC1 is dependent on binding of the KDM2B subunit to unmethylated CpG residues via a CXXC-zinc finger domain (Farcas et al., 2012; He et al., 2013; Wu et al., 2013). Interestingly, a chromatin immunoprecipitation sequencing (ChIP-seq) analysis of KDM2B demonstrated occupancy, albeit at a reduced level, at all CGIs, including those associated with active genes (Farcas et al., 2012). Based on these findings, we have proposed that PcG complexes bind CGIs as a default, with patterns of occupancy being defined on the one hand through reinforcement by positive-feedback mechanisms, and on the other hand by antagonizing chromatin modifications (e.g., H3K4me3 mediated by Trithorax group factors) at CGIs of active genes (Klose et al., 2013).

Here, we show that both PRC1 and PRC2 activities are redirected to noncanonical targets, PCH domains, and other CpG-rich sites, notably gene exons, in embryonic stem cells (ESCs) in which DNA methylation is depleted, and that this is inhibited by the presence of preexisting histone tail modifications, notably H3K9me3 and H3K36me3. Thus, PcG occupancy patterns are a combinatorial readout of unmethylated CpG density and antagonism by specific chromatin modifications. We find that tethering PRC1 proteins to PCH in wild-type (WT) cells is sufficient to establish both H2AK119u1 and PRC2-mediated H3K27me3. Moreover, we show that the observed PRC2 recruitment is directly linked to deposition of H2AK119u1. These observations define a mechanism that potentially explains the recruitment of both PRC1 and PRC2 to unmethylated CpG sites in the vertebrate genome.

RESULTS

Loss of DNA Methylation Recruits PcG Complexes to PCH

PCH in mouse comprises large blocks of major and minor satellite repeat sequences (Figure S1A) in which the chromatin is modified with H3K9me3, H4K20me3, and associated binding proteins, notably heterochromatin protein 1 (Probst and Almouzni, 2011). Atypical localization of PcG complexes and associated modifications occur on paternal PCH in early embryos (Santos et al., 2005) and have been linked to absence of H3K9 methylation (Puschendorf et al., 2008). Taking into consideration emerging evidence for an antagonistic effect of DNA methylation on PcG activity (Brinkman et al., 2012; Hagarman et al., 2013; Lynch et al., 2012; Reddington et al., 2013), we speculated that programmed DNA demethylation of the paternal genome in fertilized zygotes (Mayer et al., 2000; Oswald et al., 2000) may also play a role. To test this idea, we performed an immunofluorescence (IF) analysis to detect PRC1-mediated H2AK119u1 and PRC2-mediated H3K27me3 in Dnmt1/Dnmt3a/Dnmt3b triple knockout (Dnmt TKO) embryonic stem cells (ESCs), in which DNA methylation is depleted to 0.1%–0.4% of the levels seen in WT cells (Tsumura et al., 2006). We observed both H2AK119u1 and H3K27me3 foci colocalizing with DAPI-dense PCH domains in a large proportion of Dnmt TKO, but not WT, ESCs (Figures 1A, 1B, and S1B), demonstrating that CpG hypomethylation is sufficient to recruit PcG complexes. An unbiased quantitative analysis revealed that Dnmt TKO ESCs have a significant enrichment of H3K27me3 and H2AK119u1 in DAPI-dense domains relative to the whole nucleus (Figure 1C). A western blot analysis indicated that the global levels of PcG proteins and associated histone modifications were similar in WT and Dnmt TKO ESCs (Figure S1C).

We determined the kinetics of H3K27me3 and H2AK119u1 deposition at PCH domains using ESCs with a tamoxifen-inducible knockout allele for Uhrf1, a factor required for the maintenance of DNA methylation (Sharif et al., 2007). Similarly to Dnmt TKO ESCs, both H3K27me3 and H2AK119u1 localized to PCH in constitutive Uhrf1$^{-/-}$ ESCs, but not in Uhrf1$^{flox/flox}$ controls (Figures S2A and S2B). We therefore treated Uhrf1$^{flox/flox}$ ESCs with tamoxifen and assayed depletion of DNA methylation at major satellite repeats by Southern blot (Figure 2A), and acquisition of H3K27me3 and H2AK119u1 at PCH by IF (Figure 2B) over time. The results demonstrate a close correlation between the rate of depletion of DNA methylation and the deposition of H3K27me3/H2AK119u1 at PCH (Figure 2C). We obtained similar findings using a tamoxifen-inducible knockout ESC model for the maintenance DNA methyltransferase Dnmt1 (Figures S2C and S2D). These findings substantiate that DNA hypomethylation results in H3K27me3/H2AK119u1 deposition at PCH in ESCs, and moreover suggest a direct causative link.

We also analyzed Dnmt1$^{-/-}$ mouse embryonic fibroblasts (MEFs), which were previously shown to be extensively depleted of DNA methylation (Lande-Diner et al., 2007), to determine whether localization of H2AK119u1 and H3K27me3 to PCH occurs in a differentiated cell type. As illustrated in Figure 2D, H2AK119u1 was indeed found at PCH, but, interestingly, H3K27me3 foci were not detectable (Figure 2D). This observation indicates that PCH domains in differentiated cells have distinct characteristics (also see below).

H3K9me3 at PCH Antagonizes PRC2, but Not PRC1, Activity

Although both H3K27me3 and H2AK119u1 were seen at PCH in DNA methylation-depleted ESCs, we noted that the frequency of H3K27me3 foci was lower than the H2AK119u1 foci (Figures S3A and S3B), indicating that PCH may be somewhat refractory to PRC2 activity. Previous studies noted the appearance of H3K27me3 at PCH when H3K9me3, a histone tail modification that is normally concentrated at these sites, is depleted (Peters et al., 2003; Puschendorf et al., 2008). We therefore investigated the interplay between H3K9me3 and both H3K27me3 and H2AK119u1 in methylation-deficient Dnmt TKO compared with WT ESCs. As illustrated in Figures 3A and S3C, H2AK119u1 and HP1α (which binds to H3K9me3) show extensive overlap

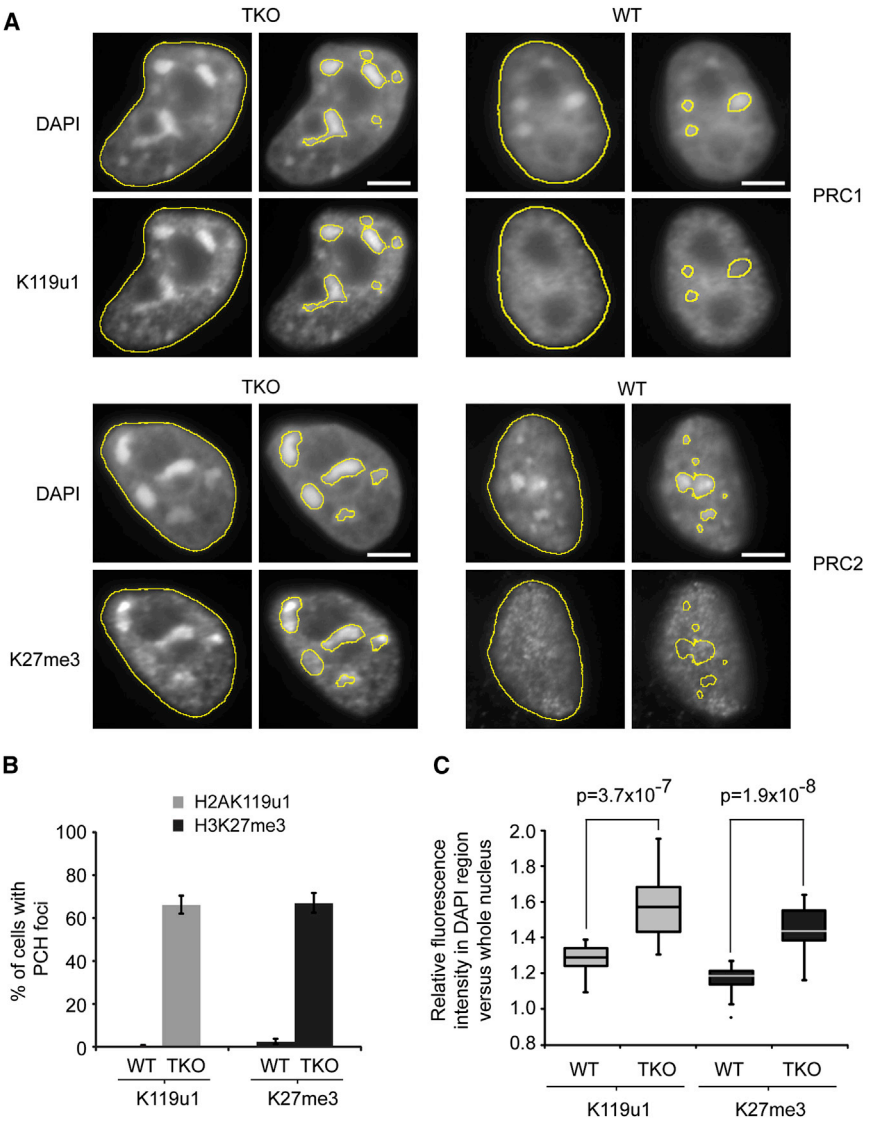

Figure 1. PcG Complexes Localize to PCH in Response to Loss of DNA Methylation

(A) IF of Dnmt TKO and WT cells stained for H2AK119u1 (PRC1) or H3K27me3 (PRC2), and DNA stained with DAPI. Yellow lines show total nuclear area (left) and PCH domains (right) based on DAPI staining defined by the ImageJ threshold algorithm Triangle.

(B) Graph showing the percentage of cells with PCH foci positive for H2AK119u1 or H3K27me3 in WT or Dnmt TKO cells. Bars show average (n > 200 DAPI foci) ± SD (n = 3).

(C) Box and whisker plot showing quantification of fluorescence intensities at PCH domains. The total nuclear area and PCH domains were defined as shown by the yellow lines in (A). Fluorescence intensity (H2AK119u1 or H3K27me3 staining) was calculated within the defined PCH domains in either WT or Dnmt TKO cells and is expressed relative to the fluorescence intensity within the total nuclear area of the cell (n = 20, p values Student's t test, unpaired).

Scale bars represent 5 μm. See also Figure S1.

with one another, encompassing the entire PCH domains. In contrast, H3K27me3 and H3K9me3 appear nonoverlapping, although both lie within DAPI-stained PCH domains (Figure 3B). We verified these observations using superresolution 3D structured illumination microscopy (3D-SIM), a technique that offers significantly enhanced spatial resolution compared with conventional fluorescence microscopy (Schermelleh et al., 2010). Representative examples shown in Figure 3C illustrate that in Dnmt TKO ESCs, H3K27me3 and H3K9me3 are enriched in distinct subdomains within PCH clusters.

The mutually exclusive deposition of H3K9me3 and H3K27me3 at PCH foci in ESCs suggests that these histone modifications may antagonize one another. Consistent with this, H3K27me3 foci in Suv3-9h1/h2 double knockout (DKO) ESCs, in which H3K9me3 at PCH is entirely depleted (Peters et al., 2001), were more extensive than in DNA methylation-depleted Dnmt TKO ESCs (Figure S3D). Moreover, in contrast to Dnmt TKO ESCs, H3K27me3 in Suv3-9h1/h2 DKO ESCs was detected in the majority of PCH domains, again similar to what was observed for H2AK119u1 (Figure S3E). To further investigate the apparent antagonism of H3K27me3 by H3K9me3, we used RNAi to deplete Suv3-9h1/h2 (and hence H3K9me3) in DNA methylation-depleted (Uhrf1$^{-/-}$) ESCs (Figure S3F), and then analyzed H3K27me3 at PCH. The extent of H3K27me3 domains was clearly increased in Suv3-9h1/h2 knockdown cells (Figure 3D), as was their frequency (Figure 3E). Moreover, we observed extensive H3K27me3 and H2AK119u1 domains in WT ESCs following Suv3-9h1/h2 depletion (Figure S3G). Taken together, these results indicate that H3K9me3 and H3K27me3 modifications are mutually antagonistic at PCH domains in ESCs.

Unmethylated CpG Titrates PcG Complexes

We went on to investigate PcG localization genome-wide following depletion of DNA methylation by performing a ChIP-seq analysis of H3K27me3, Suz12 (a core subunit of PRC2), and Ring1B (the catalytic subunit of PRC1) in Dnmt TKO and WT ESCs. Determination of the fold change in Dnmt1 TKO compared with WT ESCs at repetitive sequences, which collectively comprise approximately 45% of the genome, demonstrated enhanced levels of H3K27me3, Suz12, and Ring1B at major satellite sequences and, to a lesser extent, at minor satellite sequences (Table S1; Figure 4A), consistent with the IF data. Other common repeat sequence classes showed minimal fold changes, with a moderate reduction of H3K27me3 at L1 repeats and a slight increase of H3K27me3, Suz12, and Ring1B at SINE repeats (Figure 4A).

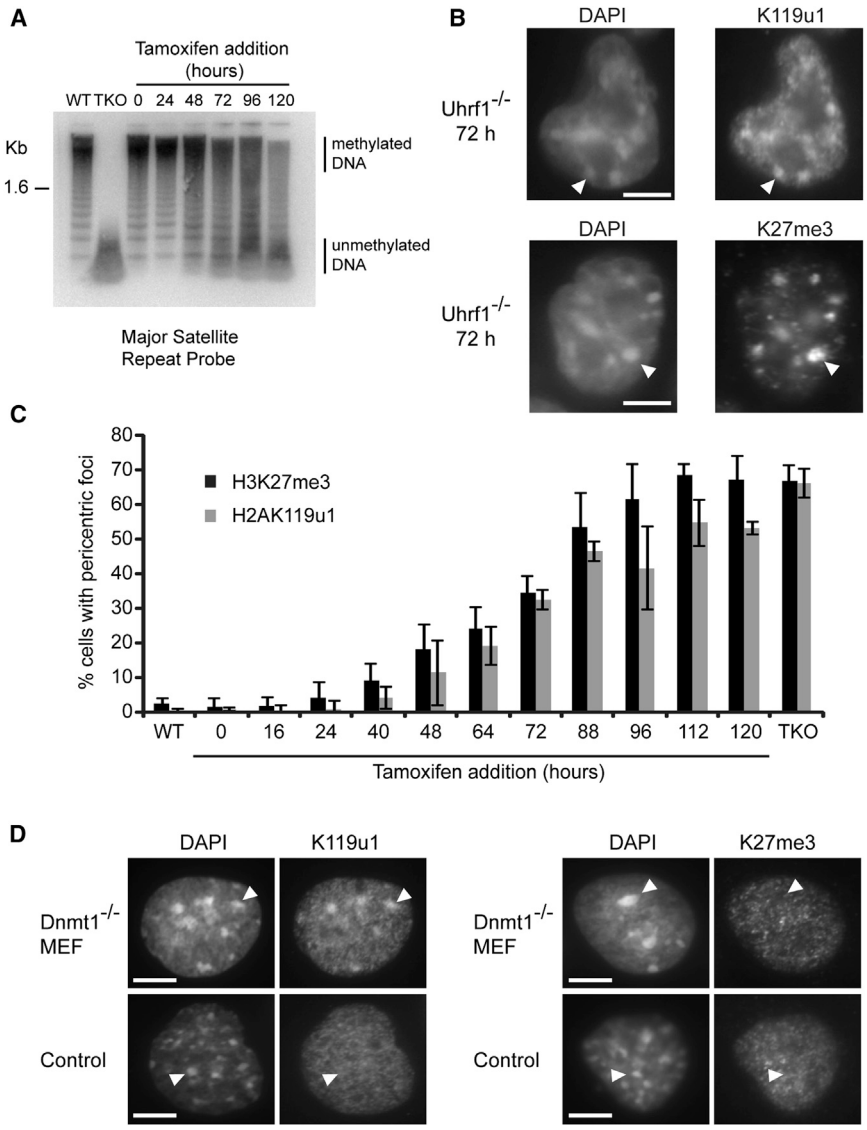

Figure 2. PcG Complexes Are Dynamically Acquired at PCH upon Loss of DNA Methylation

(A) Southern blot showing loss of DNA methylation over time upon loss of Uhrf1. Genomic DNA from WT, Dnmt TKO, or tamoxifen-induced deletion of Uhrf1 in conditional knockout cells (0–120 hr) was digested with the methylation-sensitive enzyme HpyCH41V and the blot was probed for major satellite repeats.

(B) IF of conditional knockout Uhrf1$^{-/-}$ cells (72 hr, tamoxifen treatment) stained for H2AK119u1 or H3K27me3. Arrowheads indicate an example of staining within PCH.

(C) Graph showing the percentage of cells with H3K27me3 or H2AK119u1 foci during the Uhrf1$^{-/-}$ deletion time course. Bars show average (n > 200 cells) ± SD (n = 3).

(D) IF of Dnmt1$^{-/-}$ (and control) MEF cells stained for H2AK119u1 and H3K27me3. Arrowheads indicate a single PCH domain.

Scale bars represent 5 μm. See also Figure S2.

Recent genome-wide studies have reported aberrant H3K27me3 localization at unique sequences in DNA methylation-deficient ESCs. Specifically, decreased levels occurred at CGIs of canonical PcG target loci (Brinkman et al., 2012; Reddington et al., 2013) and increased levels occurred at sites where DNA methylation levels were relatively high, notably in gene-rich chromosomal domains (Brinkman et al., 2012; Hagarman et al., 2013; Lynch et al., 2012; Reddington et al., 2013). We hypothesized that these opposite effects could be attributable to a titration of PcG complexes to newly acquired unmethylated CpG sites, including major satellite sequences, leading to a reduction in levels at canonical target sites. To investigate this, we first quantified PcG localization at canonical target loci by determining the fold change in Dnmt TKO relative to WT at known CGIs, as defined by biotin CXXC affinity purification sequencing (BioCAP-seq) experiments (Long et al., 2013b). Consistent with previous studies (Brinkman et al., 2010; Reddington et al., 2013), we observed that Dnmt TKO ESCs had reduced levels of H3K27me3, Ring1B, and Suz12 at WT PcG sites (Figure 4B). An example of a single PcG target locus, the Gata6 gene, is shown in Figure 4C, and further validation using ChIP-qPCR for H3K27me3 and H2AK119u1 at selected loci is shown in Figure 4D. We next determined the relationship between PcG occupancy and CpG density at non-CGI sequences by performing a whole-genome sliding-window analysis. We excluded embryonic, somatic, and germ cell CGIs as defined by BioCAP-seq analyis of ESCs, liver, and testis (Long et al., 2013b). Figure 4E shows a positive fold change (new sites) for non-BioCAP-seq regions binned according to CpG content, and reveals a striking correlation between the fold increase for H3K27me3 and the overall CpG content. Such a fold increase, albeit less pronounced, was also seen for Suz12 and Ring1B. We validated increased H3K27me3 at selected new sites by conventional ChIP and also demonstrated a similar increase in H2AK119u1 (Figure 4D). Taken together, these observations support the idea that unmethylated CpG sites are a primary determinant of PcG occupancy in Dnmt TKO ESCs.

A previous analysis of methylation-deficient ESCs documented a gain of H3K27me3 over large gene-rich chromosomal domains (Brinkman et al., 2012). We considered that this could be linked to the higher CpG density that has been reported to occur in gene exons (Lander et al., 2001). Importantly, we determined that the high CpG content of exons is evident even when exon 1, which frequently overlaps with promoter-associated CGIs, is excluded (4.9% CpG compared with 1.8% in introns). We therefore analyzed the fold change in H3K27me3, Suz12,

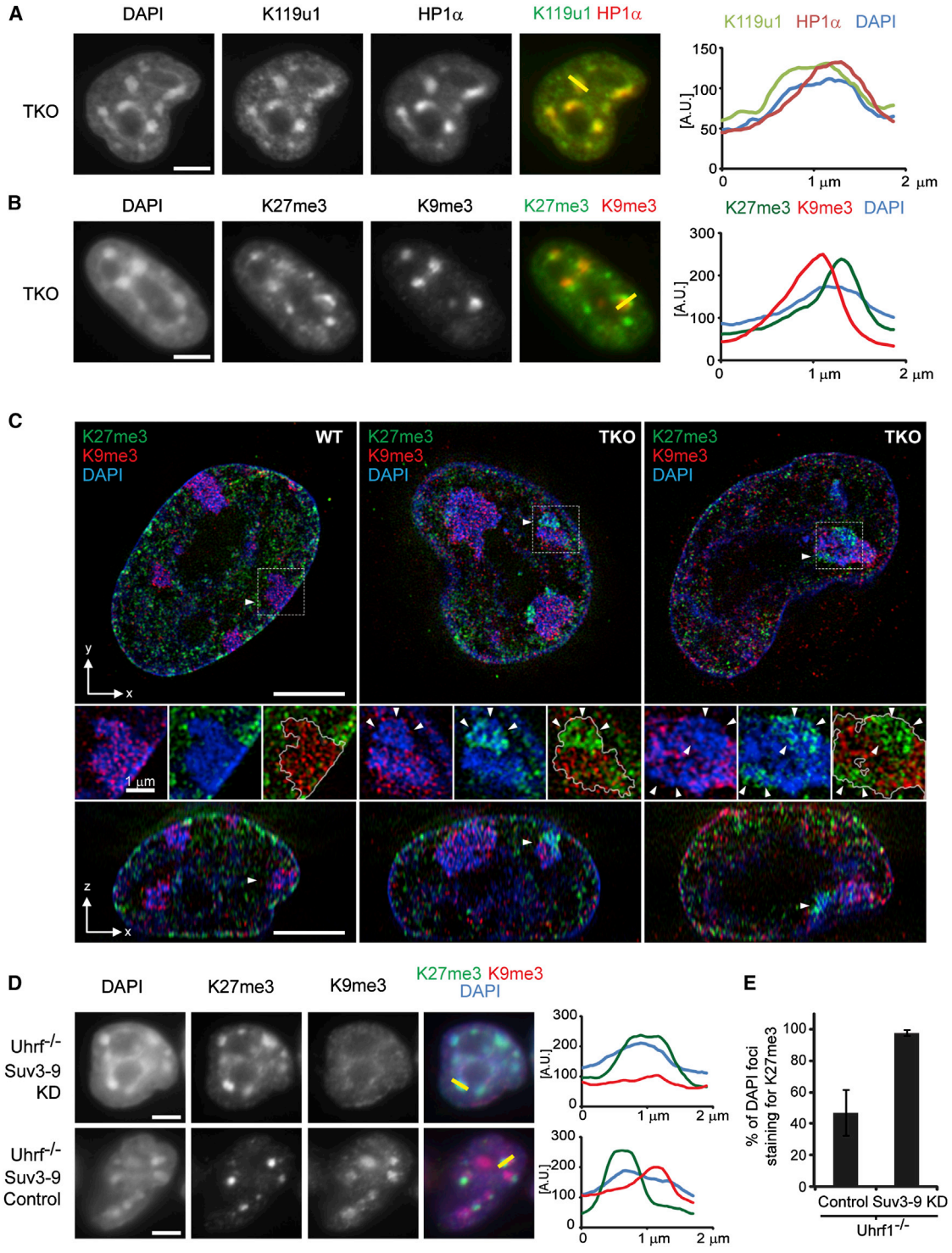

Figure 3. H3K9me3 Antagonizes PRC2, but Not PRC1

(A) IF of Dnmt TKO cells costained for H2AK119u1 and HP1α. The graph shows a profile plot of fluorescence intensity (arbitrary units [A.U.]) across a single PCH domain (2 μM) defined by DAPI and marked on the merge image as a yellow bar.

(B) As in (A), but costained for H3K27me3 and H3K9me3.

(C) Superresolution 3D-SIM images of Dnmt TKO and WT cells stained with H3K27me3 (green), H3K9me3 (red), and DAPI (blue). Upper panels show a single xy plane and bottom panels show an orthogonal xz plane. Arrowheads indicate the cutting plane. Middle panels show a single PCH region (delineated with a white line), and merges show overlap of each color. Arrowheads mark H3K27me3 staining within PCH in Dnmt TKO cells.

(legend continued on next page)

and Ring1B in Dnmt TKO relative to WT ESCs for gene exons (not exon 1) and for introns. As shown in Figure S4A, exons (excluding exon 1), but not introns, show clearly increased H3K27me3 and, to a lesser extent, Ring1B and Suz12 levels, correlating with their relative CpG content.

In vitro analysis has shown that PRC2-mediated H3K27me3 is inhibited when H3K36me2/3 is present on the same H3 tail (Schmitges et al., 2011; Yuan et al., 2011). Given that H3K36me3 is normally associated with the gene bodies of actively transcribed genes, we obtained H3K36me3 profiles for Dnmt TKO ESCs, defined H3K36me3-positive and -negative exons (not exon 1) (Figures S4B–S4D), and then determined PcG acquisition for these two exon categories in Dnmt TKO relative to WT. Consistent with the inhibitory effect of H3K36me3 on PRC2 activity, we observed little or no fold increase of H3K27me3 or the PRC2 subunit Suz12 at H3K36me3-positive exons, despite their high CpG content (4.7%) (Figure 4F). A similar effect was observed for Ring1B. We conclude that PcG redistribution at unique sequences in Dnmt TKO ESCs is a combinatorial readout of the density of unmethylated CpG density coupled to antagonism of PRC2 by H3K36me3 in the gene bodies of active genes.

PRC1 and PRC2 Activity Is Not Dependent on DNA Hypomethylation

Previous studies provided evidence for a direct effect of DNA methylation on binding/recruitment of PRC2 (Bartke et al., 2010; Wu et al., 2010). To investigate this, we assayed the activity of PRC2 (comprising the core subunits Ezh2, Eed, Suz12, and RbAp48) in vitro using chromatin templates reconstituted on a 601 nucleosome positioning sequence with a CpG density of 8.7%, which is similar to that of a CGI (Figures 5A and S5A). To verify the assay conditions, we confirmed that recombinant PRC2 was inhibited using an unmethylated DNA template and nucleosomes reconstituted with H3Kc36me3, relative to unmodified H3, as previously shown (Schmitges et al., 2011; Figure 5B, left panels). We then determined activity using either unmethylated or methylated DNA templates. As shown in Figure 5B (right panels), there was no discernible inhibition of PRC2 using the methylated template. Similarly, H2A ubiquitylation activity in vitro, assayed using a recombinant PRC1 complex comprising Ring1B, Mel-18, and Rybp (Tavares et al., 2012), was unaffected by DNA methylation (Figure 5C). These experiments argue against a direct effect of DNA methylation on the activity of the tested PRC1 and PRC2 complexes.

We went on to determine whether DNA methylation directly inhibits PcG activity in vivo. To that end, we made use of the MBD1 methyl binding domain (MBD), which binds to densely methylated DNA, including at PCH domains (Hendrich and Bird, 1998; Ng et al., 2000), to tether PcG complexes in WT ESCs with normal levels of DNA methylation (Figure 5D). In initial experiments, we constructed MBD fusion proteins for Ezh2 and Ring1B, the catalytic subunits of PRC2 and PRC1, respectively (Figure 5A). Expression of full-length fusion protein was validated by western blot analysis (Figure S5B). IF with anti-FLAG demonstrated localization of fusion proteins to PCH domains following transient transfection (Figures 5E–5G). The MBD-Ezh2 fusion protein was active, as indicated by the establishment of H3K27me3 at PCH domains (Figure 5E). Similarly, recruitment of an MBD-Ring1B fusion protein to methylated PCH domains in WT ESCs led to H2AK119u1 deposition (Figure 5F). These results argue that CpG methylation does not directly inhibit the activity of either PRC2 or PRC1 complexes.

Establishment of H3K27me3 at PCH by tethering MBD-Ezh2 did not lead to recruitment of H2AK119u1 (Figure 5G). This was unexpected given the prevailing view that H3K27me3 recruits canonical PRC1 complexes via interaction with the chromodomain of the CBX subunit. To test whether the absence of H2AK119u1 is attributable to inhibition of PRC1 activity or recruitment, we transfected either MBD-Ring1B or MBD-Ezh2 into cells stably expressing the canonical PRC1 subunit Cbx7 fused to GFP (GFP-Cbx7). Cbx7-GFP was recruited to PCH when we tethered MBD-Ring1B (because both subunits are in the same complex), but not in response to tethering of MBD-Ezh2 (Figure S5C). We conclude that the chromatin features of PCH in ESCs block binding of Cbx PcG proteins and hence canonical PRC1 to H3K27me3. This contrasts with CGI PcG target sites where H3K27me3 does recruit Cbx-PRC1 (Tavares et al., 2012). Interestingly, MBD-Ezh2 tethering to PCH in MEF cells did not result in H3K27me3 deposition (Figure 5H). This is consistent with the absence of PRC2-mediated H3K27me3 at PCH domains in Dnmt1$^{-/-}$ MEFs (Figure 2D) and indicates that PCH in differentiated MEFs is entirely refractory to PRC2 activity.

KDM2B Recruitment Is Sufficient for H2AK119u1 and H3K27me3 Deposition at PCH

In light of our observations indicating that DNA methylation does not antagonize PcG activity directly, we went on to investigate possible indirect mechanisms. Recent studies have revealed that the zinc finger CXXC (zf-CXXC) domain recruits specific chromatin-modifying factors to CGIs via binding to unmethylated CpG (Long et al., 2013a). One of these factors, KDM2B, is an H3K36me1/2 demethylase that is also a subunit of a variant PRC1 complex, PCGF1-PRC1 (Farcas et al., 2012; He et al., 2013; Wu et al., 2013). We therefore exploited the MBD fusion tethering assay described above to test whether recruitment of KDM2B could account for H2AK119u1 deposition at PCH. We mutated a critical residue in the zf-CXXC domain of KDM2B (Figure 6A) such that the fusion protein could bind to methylated, but not unmethylated, CpG. We found that MBD-KDM2B recruitment was sufficient for H2AK119u1 deposition at PCH (Figures 6B, left, and 6E). Interestingly, we also observed H3K27me3 deposition (Figure 6B, right, and 6E), albeit in a smaller

(D) Stable knockdown of Suv3-9h1/h2 or a scrambled control in Uhrf1$^{-/-}$ cells costained for H3K27me3 and H3K9me3. Profile plots as in (A) across a single PCH domain, marked on the merge image as a yellow bar.

(E) Graph showing the percentage of DAPI foci staining for H3K27me3 in Uhrf1$^{-/-}$ cells with either scrambled control or stable knockdown (KD) of Suv3-9h1/h2. Bars show average (n > 200 DAPI foci) ± SD (n = 3).

Scale bars represent 5 μm (unless otherwise stated). See also Figure S3 and Table S2.

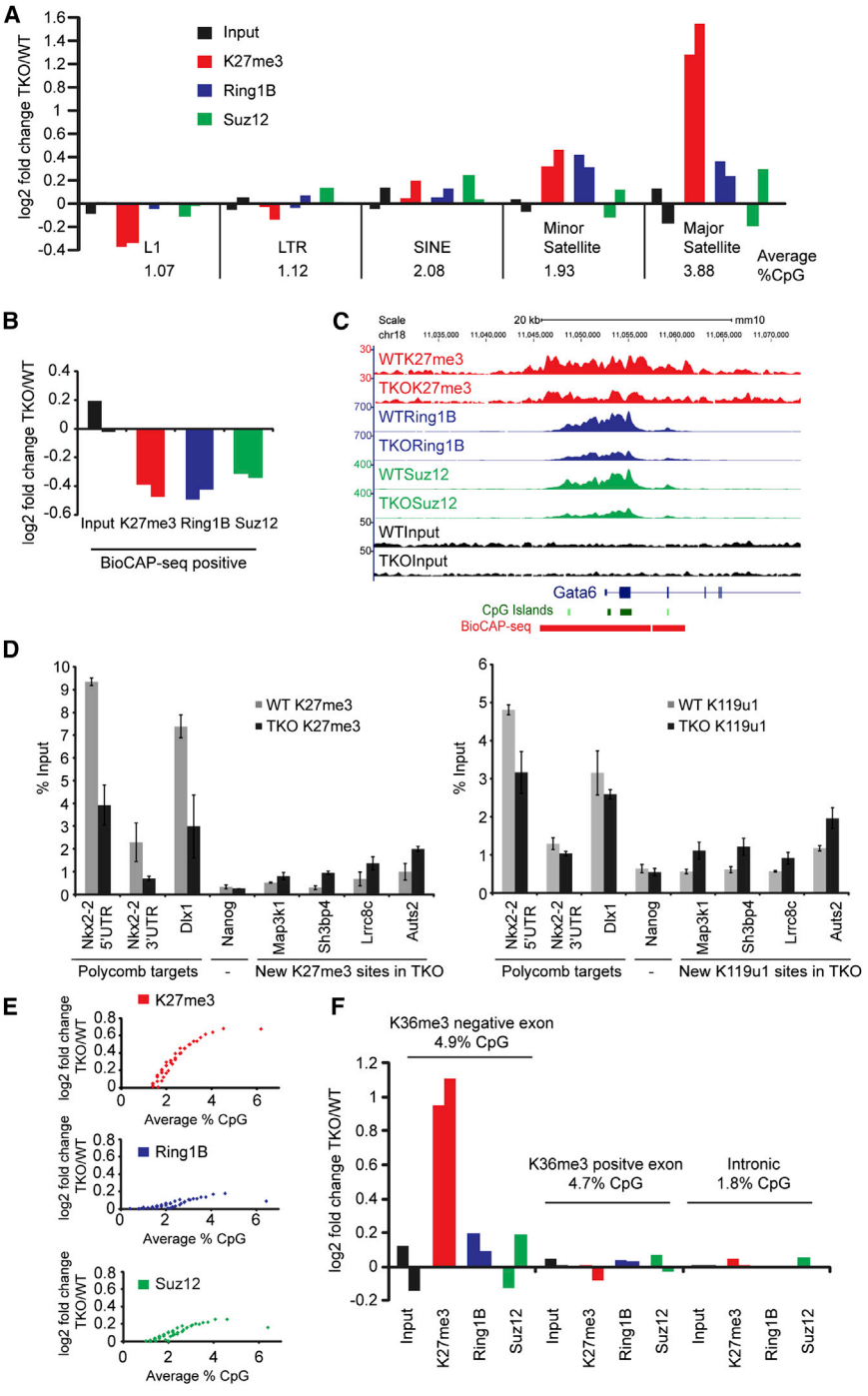

Figure 4. Loss of DNA Methylation Redistributes PcG Complexes Away from Canonical Sites to New Sites Depending on CpG Content and H3K36me3 Occupancy

(A) Graph showing at the indicated repeat regions the fold change of reads, normalized to total reads, from ChIP-seq analysis of Input, H3K27me3, Ring1B, and Suz12 in Dnmt TKO relative to WT cells. The %CpG of each repeat class is shown. Two bars represent biological repeats.

(B) As in (A), but with fold change at BioCAP-seq positive regions (WT unmethylated CpG regions).

(C) Screen shot of one biological repeat of ChIP-seq of H3K27me3, Ring1B, Suz12, and Input in WT and Dnmt TKO cells.

(D) ChIP-qPCR of H3K27me3 or H2AK119u1 at canonical targets or new sites in WT and Dnmt TKO cells. Bars show average ± SD (n = 3).

(E) Graphs showing a positive fold change in Dnmt TKO versus WT cells using a sliding-window analysis of H3K27me3, Ring1B, and Suz12 ChIP-seq of only BioCAP-seq-negative regions, binned according to CpG content.

(F) As in (A), but with fold change at H3K36me3-positive or -negative exons, or introns.

See also Figure S4 and Tables S1, S2, and S3.

proportion of cells. This was unexpected given that PRC2 is not known to interact with KDM2B /PCGF1-PRC1 (Farcas et al., 2012; He et al., 2013; Wu et al., 2013).

KDM2B is a histone demethylase with specificity for H3K36me1/2, a modification that, similarly to H3K4me3 and H3K36me3, inhibits PRC2 in *cis* on the same histone H3 tail in vitro (Schmitges et al., 2011). To test whether the H3K36me1/2 demethylase activity of KDM2B could account for H3K27me3 deposition, we tethered a catalytically inactive MBD-KDM2B fusion with a mutation in the JmjC domain (Figure 6A). As shown in Figures 6C and 6E, deposition of both H2AK119u1 and H3K27me3 was unaffected, indicating that the demethylase activity of KDM2B is not required for H3K27me3 deposition. Moreover, when we used the MBD domain to tether KDM2A, a closely related H3K36me1/2 demethylase that does not interact with PRC1 components (Blackledge et al., 2010; Farcas et al., 2012), we failed to observe either H2AK119u1 or H3K27me3 (Figures S6A–S6C).

To verify that tethering KDM2B is sufficient for deposition of both H2AK119u1 and H3K27me3, we established a stable ESC line with a doxycycline-inducible MBD-KDM2B transgene (Figure S6D). Consistent with results obtained using transient transfection, we detected deposition of both H2AK119u1 and H3K27me3 at PCH domains (Figures 6F and S6E). To test whether association of KDM2B with other PRC1 subunits is required for H3K27me3 deposition, we established a stable doxycycline-inducible ESC line expressing MBD-Ring1B (Figure S6F). As illustrated in Figures 6D and 6F, MBD-Ring1B localized to PCH domains following tamoxifen induction. This resulted in deposition of H2AK119u1, as expected, but also, importantly, to deposition of H3K27me3. Thus, recruitment of either KDM2B or Ring1B to PCH domains in WT ESCs is sufficient

to establish both H2AK119u1 and H3K27me3 histone modifications.

H2AK119u1 Recruits PRC2

Recruitment of PRC2 activity by KDM2B/Ring1B could be due to a protein-protein interaction or, alternatively, to a PRC1-linked modification of underlying chromatin. We were particularly interested in determining whether H2AK119u1 might have a direct role in recruiting PRC2. To test this, we fused the RING finger domains of Ring1B and PCGF4 to generate a minimal catalytic complex that lacks the C-terminal domains required for interaction with other PRC1 subunits (Bezsonova et al., 2009). Previous studies have shown that in vitro, the two RING finger domains dimerize to form an E3 ligase with high specificity for H2AK118/9 on nucleosomal substrates (Bentley et al., 2011; Buchwald et al., 2006; Li et al., 2006). Based on the crystal structure of this complex, which shows that the C terminus of the Ring1B ring finger and the N terminus of PCGF4 ring finger are in close proximity to each other (Bentley et al., 2011), we inserted a short linker to allow expression of the E3 ligase as a single polypeptide (Figure 7A), thereby minimizing the possibility of interactions with endogenous Ring1(A/B) or Pcgf1-6 proteins in cells. Ring1B/Pcgf4 catalytic domain (RPCD) protein was tagged with glutathione S-transferase (GST), expressed, and purified from *E. coli*. We then verified RPCD activity and specificity by assaying H2A ubiquitylation on reconstituted nucleosomal templates in vitro (Figure S7A). We also designed a catalytically inactive fusion protein by mutating a critical residue in the E2 binding surface of Ring1B (I53A) and in the zinc finger of Pcgf4 (C51G) (Figures 7A and S7A).

To test RPCD in vivo, we expressed an MBD-RPCD fusion protein with a FLAG C-terminal tag in ESCs. We verified that the fusion protein did not interact with endogenous PRC1 or PRC2 proteins by conducting a coimmunoprecipitation (coIP) analysis of Rybp, which is associated in complexes with all of Pcgf1-6 (Gao et al., 2012; Tavares et al., 2012), endogenous Ring1B, and the core PRC2 subunit Suz12. As shown in Figure S7B, Rybp coimmunoprecipitated with endogenous and MBD-tagged Ring1B, but not with RPCD. Similarly, neither endogenous Ring1B nor Suz12 coimmunoprecipitated with RPCD.

We went on to establish stable doxycycline-inducible ESCs expressing either active or mutant MBD-RPCD. The expression levels following addition of doxycycline were estimated to be similar to those in the stable MBD-Ring1B cell line described above, as determined by anti-FLAG western blot analysis (Figure S7C). When MBD-RPCD was recruited to PCH domains, we observed efficient deposition of H2AK119u1 and, importantly, H3K27me3 (Figures 7B and 7C). Neither modification could be detected following recruitment of mutant RPCD (Figures 7B and 7C). Recruitment of MBD-RPCD had no discernible effect on the levels of either H3K9me3 or DNA methylation at PCH (Figures S7D and S7E). These results thus demonstrate that H2AK119u1 deposition is sufficient to recruit PRC2. We note that this mechanism could potentially explain the localization of both PRC1 and PRC2 activities at PCH and other CpG-dense sites in DNA methylation-deficient ESCs.

DISCUSSION

A Role for DNA Hypomethylation in Atypical Localization of PcG Proteins to PCH Domains

Localization of PcG complexes to paternal PCH in early mouse embryos has been attributed to the absence of H3K9me3 (Puschendorf et al., 2008). We hypothesized that DNA hypomethylation may also play a role, and consistent with this, we observed a rapid recruitment of PRC1 and PRC2 activities to PCH in ESCs following depletion of DNA methylation, despite the continued presence of H3K9me3. Our results do, however, support a role for H3K9me3 in antagonizing PRC2 activity at PCH. Specifically, we observed mutually exclusive staining for H3K9me3 and H3K27me3, contrasting with the broader staining pattern for H2AK119u1. Moreover, depletion of H3K9me3 by knockdown of Suv39h1/h2 resulted in increased H3K27me3 at PCH. H3K9me3 does not inhibit PRC2 activity in vitro (Schmitges et al., 2011), arguing against direct inhibition of PRC2 activity by H3K9me3 in *cis* on the same histone tail. With this in mind, we favor the idea that antagonism of PRC2 by H3K9me3 at PCH is an indirect effect, mediated by H3K9me3-binding proteins such as HP1.

Unlike the case with H3K27me3, H2AK119u1 deposition at PCH in Dnmt TKO ESCs is not antagonized by H3K9me3. This raises the question of how H2AK119u1 deposition at PCH occurs in Suv39H1/2 DKO ESCs. Our results suggest that H2AK119u1 deposition is unlikely to be attributable to H3K27me3-mediated recruitment of canonical PRC1 complexes, given that this does not occur when H3K27me3 is directed to PCH in WT ESCs (Figure 5G). A possible explanation comes from the observation that H3K9me3 is required for efficient DNA methylation at PCH (Lehnertz et al., 2003). Thus, DNA hypomethylation in Suv39H1/2 DKO ESCs could recruit PRC1 activity, similar to what is observed in Dnmt TKO ESCs (see below). It should be noted that the absence of canonical PRC1 recruitment at H3K27-methylated PCH is unexpected. We interpret this to indicate that Polycomb Cbx proteins are unable to bind to H3K27me3 due to a specific characteristic or modification at PCH.

We also show that PcG activity/recruitment at PCH is dependent on developmental context. Specifically, in Dnmt1$^{-/-}$ MEF cells, we observed accumulation of H2AK119u1, but never H3K27me3. This was the case even following depletion of H3K9me3 (data not shown). Related to this, in contrast to ESCs, tethering Ezh2 to PCH in WT MEFs did not lead to H3K27me3 deposition. These observations demonstrate that PCH in somatic cells is highly refractory to PRC2 activity. Inhibition of PRC2 may be linked to the fact that PCH chromatin is considerably less dynamic in somatic cells relative to ESCs (Meshorer et al., 2006). Thus, we propose interplay of mutually exclusive chromatin repression machineries, with the equilibrium state being defined in part by chromatin dynamics.

Unmethylated CpG Dictates PcG Occupancy

Our study extends recent reports of a changed distribution of H3K27me3 in DNA methylation-deficient ESCs (Brinkman et al., 2012) and somatic cell lines (Reddington et al., 2013). Specifically, we mapped H3K27me3, Suz12, and Ring1B redistribution in

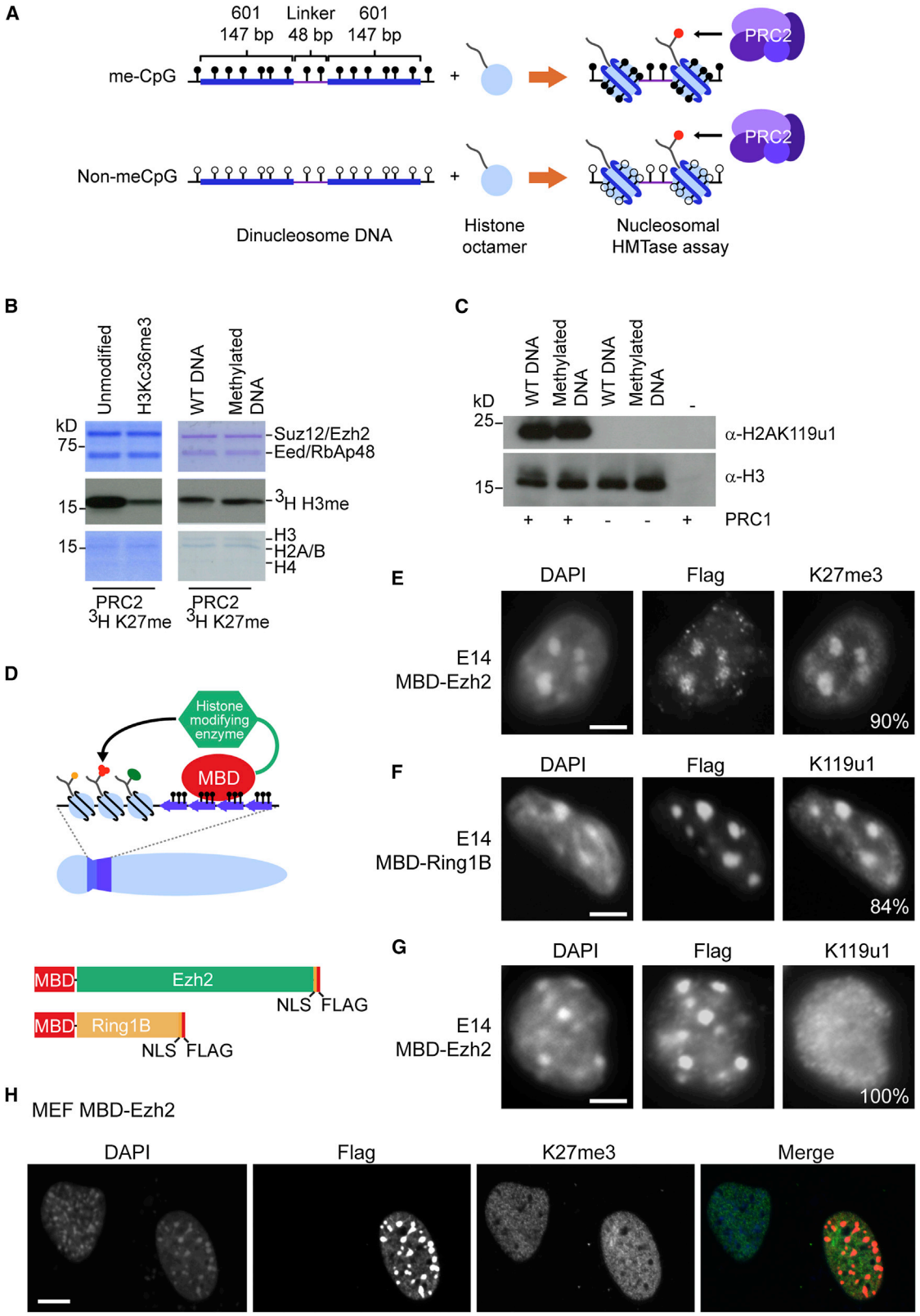

(legend on next page)

Dnmt TKO ESCs, and also performed an extended analysis to include common repeat elements. These analyses demonstrate that both PRC1 and PRC2 are redistributed away from canonical PcG targets. Moreover, by subtracting ESC PcG target sequences from our analysis, we were able to show that there is a linear relationship between the gain of PcG complexes and the density of unmethylated CpG, notably at exon sequences that are known to have a relatively high CpG density. By taking into consideration the levels of H3K36me3, which was previously shown to inhibit PRC2 activity, we further refined the principles for PcG redistribution following depletion of CpG methylation. Together, our observations indicate that PcG redistribution at unique sequences in Dnmt TKO ESCs is a combinatorial readout of the density of unmethylated CpG and the presence/absence of H3K36me3. We note that modified patterns of DNA methylation could also explain the observed changes in patterns of PcG occupancy in ESCs grown in 2i conditions (Ficz et al., 2013; Habibi et al., 2013; Marks et al., 2012), in Dnmt3a-deficient neural stem cells (Wu et al., 2010), and in cancer cell lines (Varley et al., 2013). In the context of the default model for PcG recruitment (Klose et al., 2013), we suggest that other histone tail modifications, notably H3K4me3, which antagonizes PRC2 activity, must also be taken into account in order to fully explain PcG occupancy patterns in different cell types.

Although we detected gain of both H3K27me3 and H2AK119u1 at new sites in Dnmt TKO ESCs, this was less obvious when we analyzed Suz12 and Ring1B. A possible explanation for this is that at new sites, PcG complexes interact with chromatin with relatively fast dynamics and as such evade capture by formaldehyde crosslinking (Schmiedeberg et al., 2009). Fast dynamics at the relatively short CpG-rich exonic sites could be linked to an absence of positive-feedback mechanisms that stabilize PcG complexes at CGI targets. The enhancement of PcG silencing by polymerization of the SAM domain of the Polyhomeotic subunit of canonical PRC1 complexes (Isono et al., 2013) may represent one such mechanism.

Our results support a view that PcG localization in vertebrate cells is dictated in large part by the distribution of unmethylated CpG sites. This mechanism may also operate in other organisms, such as in *A. thaliana*, where hypomethylation of DNA at transposons in a met1 mutant or endogenously in the endosperm results in PRC2 recruitment (Deleris et al., 2012; Weinhofer et al., 2010). However, this cannot account for PcG distribution patterns in *Drosophila* and *C. elegans*, where there is no DNA methylation. Nevertheless, there is an interesting parallel in *C. elegans*, where mutation of the H3K36me2/3 methyltransferase MES4 results in PRC2 relocalization from the X chromosome to autosomes in germ cells (Gaydos et al., 2012). Thus, inhibition of PRC2 by specific histone modifications could be used as an alternative mechanism to limit sites of activity and hence define patterns of occupancy of PcG complexes.

Monoubiquitylation of H2A Recruits PRC2

Our findings illustrate that unmethylated CpG is an important determinant of PcG occupancy in mammalian cells. However, although we cannot entirely rule out some contribution, we do not find evidence that this is due to direct inhibition of PRC1/2 enzymatic activity by methylated CpG. Similarly, inhibition of PRC2 by H3K36me2, as predicted on the basis of in vitro studies (Schmitges et al., 2011), does not appear to be a primary determinant of PcG localization in mammalian cells in vivo. Again, we cannot entirely rule out the possibility that H3K36me2 may have some role in limiting PRC2 activity at non-PcG target domains. Our findings do, however, support an alternative model: the sequential recruitment of variant PRC1 to unmethylated CpG, notably via binding of the CXXC domain of the KDM2B protein, and indirect recruitment of PRC2 in response to PRC1-mediated H2AK119u1. Recruitment of PRC2 in response to H2AK119u1 deposition is substantiated by the observation that acquisition of H3K27me3 at PCH shows a linear relationship with H2AK119u1, as seen in a comparison of KDM2B, Ring1B, and RPCD tethering (Figures 6 and 7). Furthermore, only catalytically active RPCD brings in H3K27me3, and in coIP experiments we did not find a direct interaction between RPCD and either PRC1 or, importantly, PRC2 subunits. This is also supported by a mass spectrometry analysis of TetR-RPCD (Blackledge et al., 2014). We found no evidence that RPCD-mediated H2AK119u1 results in DNA hypomethylation, which could potentially account for recruitment of endogenous PRC1/2 to PCH. Consistent with this, recruitment of RPCD to a TetR array that does not have any CpG sites also leads to establishment of H3K27me3 (N.P.B., A.M. Farcas, T. Kondo, H.W. King, J.F. McGouran, L.L.P. Hanssen, S. Ito, S.C., K. Kondo, Y. Koseki, T. Ishikura, H.K. Long, T.W. Sheahan, N.B., B.M. Kessler, H.K., and R.K., unpublished data).

The finding that H2AK119 ubiquitylation is sufficient to recruit PRC2 to chromatin was largely unanticipated, although, interestingly, a prior study noted a loss of H3K27me3 in Ring1A/B DKO ESCs (Endoh et al., 2008). This has been substantiated in a recent study (N.P.B., A.M. Farcas, T. Kondo, H.W. King, J.F. McGouran, L.L.P. Hanssen, S. Ito, S.C., K. Kondo, Y. Koseki, T. Ishikura, H.K. Long, T.W. Sheahan, N.B., B.M. Kessler, H.K.,

Figure 5. DNA Methylation Does Not Inhibit PcG Activity Directly

(A) Schematic showing in vitro methylation of 601 positioning DNA and reconstitution of dinucleosomes.

(B) PRC2 histone methyltransferase assay using ^{3}H SAM and either WT/H3Kc36me3 nucleosomes or WT/methylated DNA nucleosomes as substrate. Top and bottom panels: Coomassie-stained gel; middle panel: autoradiography of dried gel.

(C) PRC1 ubiquitylation assay using WT/methylated DNA nucleosomes as substrate, and analyzed by western blot (probed for H2AK119u1 or H3).

(D) Schematic of MBD tethering assay to target proteins of interest to regions of methylated DNA.

(E) MBD-Ezh2-Flag transfected into E14 ESCs stained for Flag and H3K27me3. The percentage of cells that showed the illustrated phenotype is indicated ($n > 200$).

(F) As in (E), but transfected with MBD-Ring1B-Flag and stained for Flag and H2AK119u1.

(G) As in (E), but transfected with MBD-Ezh2-Flag and stained for Flag and H2AK119u1.

(H) MBD-Ezh2-Flag transfected into MEFs and stained for Flag and H3K27me3.

Scale bars represent 5 μm. See also Figure S5.

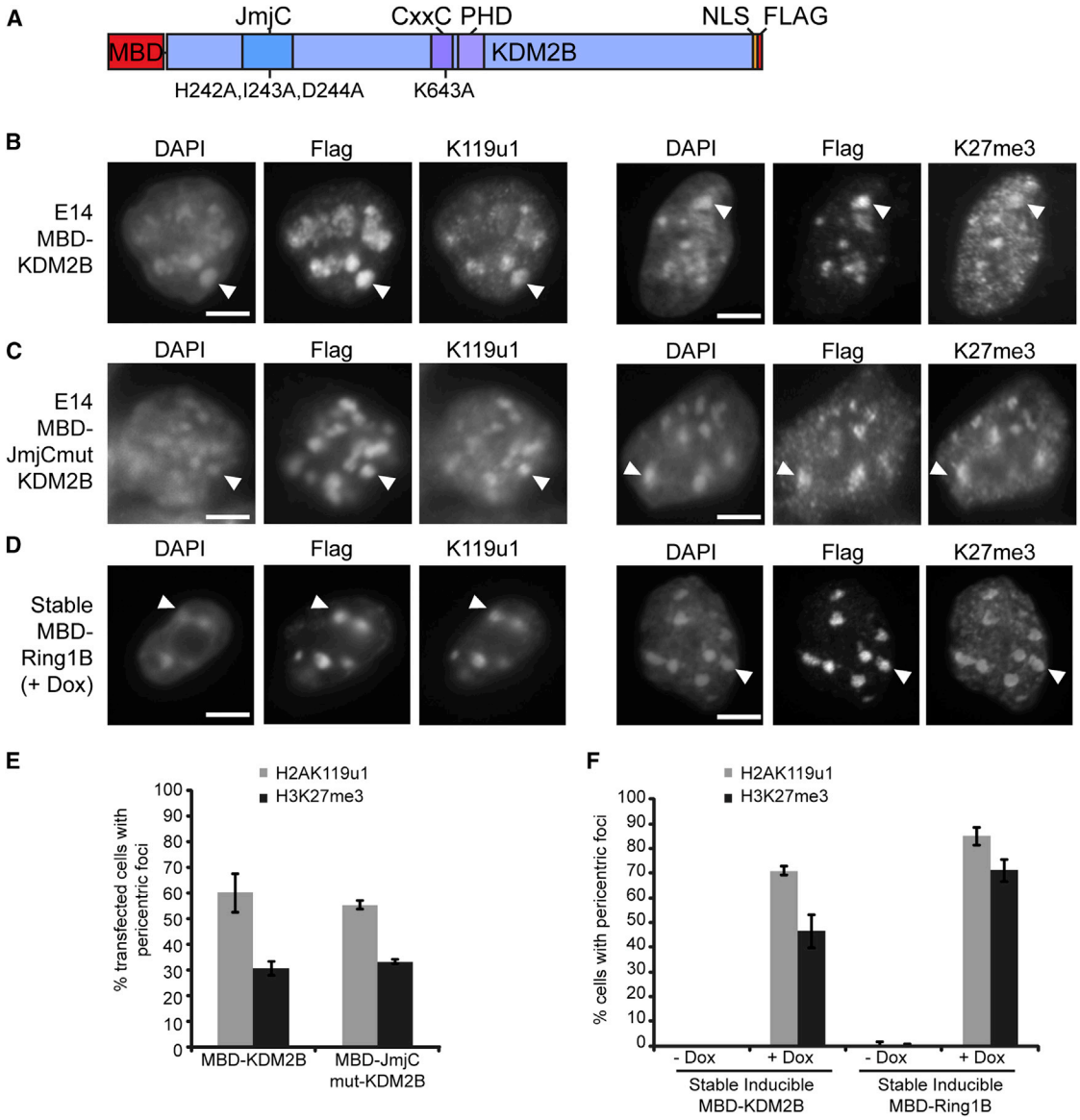

Figure 6. KDM2B and Ring1B Recruit PRC2 Activity to PCH Domains

(A) Schematic of MBD-KDM2B-Flag indicating the positions of mutations in the JmjC domain (HID-AAA) and the CxxC domain (K-A).

(B) MBD-KDM2B transfected into E14 ESCs stained for Flag and H2AK119u1 (left) and Flag and H3K27me3 (right).

(C) MBD-KDM2B-Flag catalytic mutant (JmjC mutant HID-AAA) transfected into E14 ESCs stained for Flag and H2AK119u1 (left), and Flag and H3K27me3 (right).

(D) Inducible stable line expressing MBD-Ring1B-Flag, stained for Flag and H2AK119u1 3 days after induction with doxycycline (left) and Flag and H3K27me3 (right).

(E) Graph showing the percentage of transfected cells with H2AK119u1 (gray) or H3K27me3 (black) PCH foci in cells transfected with WT MBD-KDM2B and catalytically inactive JmjC domain mutant. Bars show average ($n > 200$ transfected cells) ± SD ($n > 3$).

(F) Graph showing the percentage of cells with H2AK119u1 (gray) or H3K27me3 (black) PCH foci in stable MBD-KDM2B and stable MBD-Ring1B either with or without 3 days induction with doxycycline ($n > 100$ cells) ± SD ($n > 3$). Arrowheads indicate an example of staining within Flag domains at PCH.

Scale bars represent 5 μm. See also Figures S5 and S6.

and R.K., unpublished data). Taken together, these observations demonstrate hierarchical recruitment of PRC2 by PRC1 activity. The data are consistent with a primary role for variant PRC1 and H2AK119u1 in determining PcG target sites, although we do not rule out the possibility that PRC2 may also be recruited independently of H2AK119u1.

A key question for future studies is: what is the mechanistic basis for H2AK119u1-mediated recruitment of PRC2? One possibility is that PRC2 acts as a reader of H2AK119u1, either directly or via a cofactor that can bind the modified chromatin (see Figure 7D, top panel). Consistent with this idea, a previous study identified the ZRF1 protein as an H2AK119u1-binding

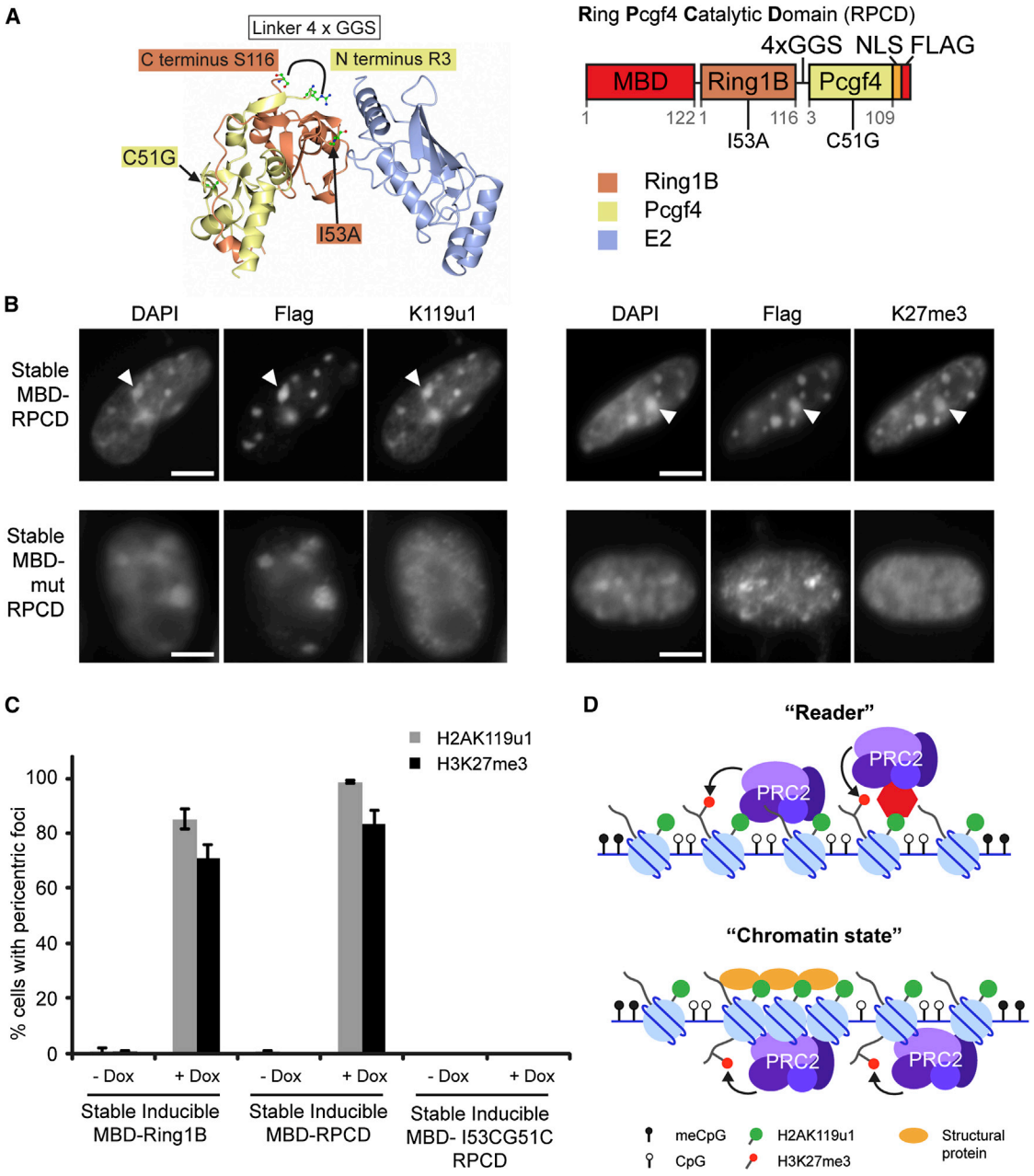

Figure 7. Ubiquitylated H2A Is Sufficient to Recruit PRC2 to PCH Domains

(A) Structure of the minimal E3 and E2 complex (Bentley et al., 2011), showing the catalytic domain of Pcgf4 (yellow) and Ring1B (orange) interacting with E2 enzyme (blue). RPCD was made by fusing the C terminus (S116) of Ring1B to the N terminus (R3) of Pcgf4 using a 4x GGS flexible linker. Catalytic mutant (mut) RPCD comprised C51G (in Pcgf4) and I53A (in Ring1B).

(B) Inducible stable line expressing MBD-RPCD-Flag or MBD-mut-RPCD-Flag, stained for Flag and H2AK119u1 3 days after induction with doxycycline (left) and Flag and H3K27me3 (right). Arrowheads indicate an example of staining within Flag domains at PCH.

(C) Graph showing the percentage of cells with H2AK119u1 (gray) or H3K27me3 (black) PCH foci in stable MBD-Ring1B-Flag, MBD-RPCD-Flag, and MBD-mut-RPCD-Flag cell lines, either with or without 3 days induction with doxycycline (n > 100 cells) ± SD (n > 3).

(D) Schematic to illustrate potential models of for PRC2 recruitment by H2AK119u1, either by direct/indirect protein interactions "reader" (top) or by "chromatin state" (bottom).

Scale bars represent 5 μm. See also Figure S7.

protein (Richly et al., 2010). Alternatively, H2AK119 ubiquitylation may affect chromatin structure in such a way as to facilitate the binding and/or activity of PRC2 complexes (Figure 7D, bottom panel). In this context, it should be noted that H2AK119u1 does not stimulate PRC2 activity on mononucleosome substrates in vitro (Whitcomb et al., 2012). Conversely, a recent

study revealed that chromatin compaction stimulates PRC2 (Yuan et al., 2012), consistent with the idea that local chromatin configuration is important.

In summary, our findings provide insights into the link between DNA methylation and PcG recruitment, and are consistent with the recently suggested model in which Polycomb recruitment in vertebrates is a default state at licensed chromatin sites, defined directly or indirectly by CpG methylation status (Klose et al., 2013).

EXPERIMENTAL PROCEDURES

ESC Culture

E14TG2A, Dnmt TKO (Dnmt1$^{-/-}$, Dnmt3a$^{-/-}$, Dnmt3b$^{-/-}$) and matched WT (J1) (Tsumura et al., 2006), conditional Uhrf1 and Dnmt1 knockout cells (Sharif et al., 2007), constitutive Suv3-9h1/h2 DKO and matched WT ESCs (Peters et al., 2003), and Dnmt1$^{-/-}$ MEFs and matched control MEFs (Lande-Diner et al., 2007) were cultivated using established methods. See also Supplemental Experimental Procedures.

Constructs

Amino acids 1–112 of human MBD1, which include the MBD domain and endogenous nuclear localization sequence (NLS) signal, followed by a glycine- and serine-rich flexible linker, were cloned to the N terminus of the protein of interest in pBluescript. An SV40 NLS, followed by a FLAG-tag, was cloned on the C terminus of the protein of interest. These MBD-fusion proteins were then cloned into the mammalian expression plasmid pCAG, in which the MBD-fusion protein was under the control of the constitutive β-actin promoter. Full-length mouse Ezh2, mouse Ring1B, and human KDM2A (K601A) and KDM2B (K643A) were targeted to methylated DNA using the MBD domain. For KDM2A/B, the CxxC DNA binding domains were mutated (K601A and K643A, respectively). The MBD-KDM2B, MBD-Ring1B, MBD-RPCD, and MBD-mutRPCD constructs were also cloned into the pTight vector to allow doxycyline-inducible expression when stably integrated into rtTA2A10 ESCs.

Amino acids 1–116 of Ring1B and 3–109 of Pcgf4 (termed Ring1b Pcgf4 catalytic domain RPCD fusion) were joined using a 4x GGS flexible linker and cloned with an N-terminal GST tag in pGex-6p2 for bacterial protein expression and purification, or with an N-terminal MBD domain in the pCAG vector, for expression in ESCs. Catalytic mutants were made in the JmjC domain of KDM2B (H242A, I243A, D244A) and in RPCD at Ring1B I53A to mutate the E2 interaction domain, and at Pcgf4 C51G to mutate the zinc finger domain, using a site-directed mutagenesis kit (Stratagene). Synthesized core PRC2 subunits (full-length EZH2, EED, SUZ12, and RbAp48) were codon optimized for expression in insect cells (GeneArt) and cloned into pBAC4x-1 (Novagen) using the In-Fusion cloning system (Clontech).

Immunofluorescence

ESCs or MEFs were split onto slides 16 hr before staining at low density (without feeders). Slides were then washed in PBS, fixed with 2% formaldehyde in PBS for 15 min, and permeabilized with 0.4% Triton X-100 in PBS for 5 min. After washing with PBS, the slides were blocked for 30 min in 0.2% fish gelatin (Sigma) in PBS and incubated for 2 hr with primary antibody (diluted in 0.2% fish gelatin and 5% normal goat serum). Slides were washed three times in 0.2% fish gelatin and incubated for 2 hr with Alexa Fluor conjugated secondary antibody (Life Technologies). After two washes in fish gelatin and two washes in PBS, the slides were stained with DAPI (1 μg/ml) and mounted using mounting media (Dako).

The following primary antibodies were used for IF: H2AK119u1 (1:500, rabbit monoclonal, 8240; Cell Signaling Technology), H3K27me3 (1:500, rabbit polyclonal, pAB-069-050; Diagenode), H3K27me3 (1:1,000, mouse monoclonal, 61017; Active Motif), Flag (1:500, mouse M2 monoclonal; Sigma), H3K9me3 (1:500, rabbit polyclonal 39161; Active Motif), H3K4me3 (1:500, rabbit polyclonal, ab8580; Abcam), HP1α (1:500, mouse monoclonal MAB3584; Millipore), and GFP (1:100, mouse monoclonal, sc-9996; Santa Cruz).

Chromatin Immunoprecipitation

ChIP/ChIP-seq was carried out as described previously (Blackledge et al., 2010). Full details are provided in the Supplemental Experimental Procedures. The antibodies for ChIP-seq were H3K27me3 (pAB-069-100; Diagenode), H3K36me3 (AB9050; Abcam), anti-Suz12 (3737S; Cell Signaling Technology), and anti-Ring1B (Atsuta et al., 2001).

ACCESSION NUMBERS

The European Nucleotide Archive accession number for the ChIP-seq data reported in this paper is ERP005575.

SUPPLEMENTAL INFORMATION

Supplemental Information includes Supplemental Experimental Procedures, seven figures, and three tables and can be found with this article online at http://dx.doi.org/10.1016/j.celrep.2014.04.012.

ACKNOWLEDGMENTS

We thank Andrew Bassett and members of the N.B. and R.K. labs for critical readings of the manuscript. We thank Masaki Okano for Dnmt TKO ESCs, Thomas Jenuwein for Suv3-9 DKO ESCs, and Howard Cedar for p-/p-m-MEFS. This work was funded by grants from the Wellcome Trust (WT081385, WT091911, and WT098024) and the Medical Research Council, UK (G1000902).

Received: November 19, 2013
Revised: March 12, 2014
Accepted: April 11, 2014
Published: May 22, 2014

REFERENCES

Atsuta, T., Fujimura, S., Moriya, H., Vidal, M., Akasaka, T., and Koseki, H. (2001). Production of monoclonal antibodies against mammalian Ring1B proteins. Hybridoma *20*, 43–46.

Bartke, T., Vermeulen, M., Xhemalce, B., Robson, S.C., Mann, M., and Kouzarides, T. (2010). Nucleosome-interacting proteins regulated by DNA and histone methylation. Cell *143*, 470–484.

Bentley, M.L., Corn, J.E., Dong, K.C., Phung, Q., Cheung, T.K., and Cochran, A.G. (2011). Recognition of UbcH5c and the nucleosome by the Bmi1/Ring1b ubiquitin ligase complex. EMBO J. *30*, 3285–3297.

Bestor, T.H. (2000). The DNA methyltransferases of mammals. Hum. Mol. Genet. *9*, 2395–2402.

Bezsonova, I., Walker, J.R., Bacik, J.P., Duan, S., Dhe-Paganon, S., and Arrowsmith, C.H. (2009). Ring1B contains a ubiquitin-like docking module for interaction with Cbx proteins. Biochemistry *48*, 10542–10548.

Blackledge, N.P., Zhou, J.C., Tolstorukov, M.Y., Farcas, A.M., Park, P.J., and Klose, R.J. (2010). CpG islands recruit a histone H3 lysine 36 demethylase. Mol. Cell *38*, 179–190.

Blackledge, N.P., Farcas, A.M., Kondo, T., King, H.W., McGouran, J.F., Hanssen, L.L.P., Ito, S., Cooper, S., Kondo, K., Koseki, Y., et al. (2014). Variant PRC1 complex-dependent H2A ubiquitylation drives PRC2 recruitment and polycomb domain formation. Cell *157*, 1445–1459.

Brinkman, A.B., Simmer, F., Ma, K., Kaan, A., Zhu, J., and Stunnenberg, H.G. (2010). Whole-genome DNA methylation profiling using MethylCap-seq. Methods *52*, 232–236.

Brinkman, A.B., Gu, H., Bartels, S.J., Zhang, Y., Matarese, F., Simmer, F., Marks, H., Bock, C., Gnirke, A., Meissner, A., and Stunnenberg, H.G. (2012). Sequential ChIP-bisulfite sequencing enables direct genome-scale investigation of chromatin and DNA methylation cross-talk. Genome Res. *22*, 1128–1138.

Brockdorff, N. (2013). Noncoding RNA and Polycomb recruitment. RNA *19*, 429–442.

Buchwald, G., van der Stoop, P., Weichenrieder, O., Perrakis, A., van Lohuizen, M., and Sixma, T.K. (2006). Structure and E3-ligase activity of the Ring-Ring complex of polycomb proteins Bmi1 and Ring1b. EMBO J. *25*, 2465–2474.

Cao, R., Wang, L., Wang, H., Xia, L., Erdjument-Bromage, H., Tempst, P., Jones, R.S., and Zhang, Y. (2002). Role of histone H3 lysine 27 methylation in Polycomb-group silencing. Science *298*, 1039–1043.

de Napoles, M., Mermoud, J.E., Wakao, R., Tang, Y.A., Endoh, M., Appanah, R., Nesterova, T.B., Silva, J., Otte, A.P., Vidal, M., et al. (2004). Polycomb group proteins Ring1A/B link ubiquitylation of histone H2A to heritable gene silencing and X inactivation. Dev. Cell *7*, 663–676.

Deleris, A., Stroud, H., Bernatavichute, Y., Johnson, E., Klein, G., Schubert, D., and Jacobsen, S.E. (2012). Loss of the DNA methyltransferase MET1 Induces H3K9 hypermethylation at PcG target genes and redistribution of H3K27 trimethylation to transposons in Arabidopsis thaliana. PLoS Genet. *8*, e1003062.

Endoh, M., Endo, T.A., Endoh, T., Fujimura, Y., Ohara, O., Toyoda, T., Otte, A.P., Okano, M., Brockdorff, N., Vidal, M., and Koseki, H. (2008). Polycomb group proteins Ring1A/B are functionally linked to the core transcriptional regulatory circuitry to maintain ES cell identity. Development *135*, 1513–1524.

Endoh, M., Endo, T.A., Endoh, T., Isono, K., Sharif, J., Ohara, O., Toyoda, T., Ito, T., Eskeland, R., Bickmore, W.A., et al. (2012). Histone H2A mono-ubiquitination is a crucial step to mediate PRC1-dependent repression of developmental genes to maintain ES cell identity. PLoS Genet. *8*, e1002774.

Eskeland, R., Leeb, M., Grimes, G.R., Kress, C., Boyle, S., Sproul, D., Gilbert, N., Fan, Y., Skoultchi, A.I., Wutz, A., and Bickmore, W.A. (2010). Ring1B compacts chromatin structure and represses gene expression independent of histone ubiquitination. Mol. Cell *38*, 452–464.

Farcas, A.M., Blackledge, N.P., Sudbery, I., Long, H.K., McGouran, J.F., Rose, N.R., Lee, S., Sims, D., Cerase, A., Sheahan, T.W., et al. (2012). KDM2B links the Polycomb Repressive Complex 1 (PRC1) to recognition of CpG islands. Elife *1*, e00205.

Ficz, G., Hore, T.A., Santos, F., Lee, H.J., Dean, W., Arand, J., Krueger, F., Oxley, D., Paul, Y.L., Walter, J., et al. (2013). FGF signaling inhibition in ESCs drives rapid genome-wide demethylation to the epigenetic ground state of pluripotency. Cell Stem Cell *13*, 351–359.

Francis, N.J., Kingston, R.E., and Woodcock, C.L. (2004). Chromatin compaction by a polycomb group protein complex. Science *306*, 1574–1577.

Gao, Z., Zhang, J., Bonasio, R., Strino, F., Sawai, A., Parisi, F., Kluger, Y., and Reinberg, D. (2012). PCGF homologs, CBX proteins, and RYBP define functionally distinct PRC1 family complexes. Mol. Cell *45*, 344–356.

Gaydos, L.J., Rechtsteiner, A., Egelhofer, T.A., Carroll, C.R., and Strome, S. (2012). Antagonism between MES-4 and Polycomb repressive complex 2 promotes appropriate gene expression in *C. elegans* germ cells. Cell Rep *2*, 1169–1177.

Habibi, E., Brinkman, A.B., Arand, J., Kroeze, L.I., Kerstens, H.H., Matarese, F., Lepikhov, K., Gut, M., Brun-Heath, I., Hubner, N.C., et al. (2013). Whole-genome bisulfite sequencing of two distinct interconvertible DNA methylomes of mouse embryonic stem cells. Cell Stem Cell *13*, 360–369.

Hagarman, J.A., Motley, M.P., Kristjansdottir, K., and Soloway, P.D. (2013). Coordinate regulation of DNA methylation and H3K27me3 in mouse embryonic stem cells. PLoS ONE *8*, e53880.

He, J., Shen, L., Wan, M., Taranova, O., Wu, H., and Zhang, Y. (2013). Kdm2b maintains murine embryonic stem cell status by recruiting PRC1 complex to CpG islands of developmental genes. Nat. Cell Biol. *15*, 373–384.

Hendrich, B., and Bird, A. (1998). Identification and characterization of a family of mammalian methyl-CpG binding proteins. Mol. Cell. Biol. *18*, 6538–6547.

Illingworth, R.S., and Bird, A.P. (2009). CpG islands—'a rough guide'. FEBS Lett. *583*, 1713–1720.

Isono, K., Endo, T.A., Ku, M., Yamada, D., Suzuki, R., Sharif, J., Ishikura, T., Toyoda, T., Bernstein, B.E., and Koseki, H. (2013). SAM domain polymerization links subnuclear clustering of PRC1 to gene silencing. Dev. Cell *26*, 565–577.

Kassis, J.A., and Brown, J.L. (2013). Polycomb group response elements in Drosophila and vertebrates. Adv. Genet. *81*, 83–118.

Klose, R.J., Cooper, S., Farcas, A.M., Blackledge, N.P., and Brockdorff, N. (2013). Chromatin sampling—an emerging perspective on targeting polycomb repressor proteins. PLoS Genet. *9*, e1003717.

Lande-Diner, L., Zhang, J., Ben-Porath, I., Amariglio, N., Keshet, I., Hecht, M., Azuara, V., Fisher, A.G., Rechavi, G., and Cedar, H. (2007). Role of DNA methylation in stable gene repression. J. Biol. Chem. *282*, 12194–12200.

Lander, E.S., Linton, L.M., Birren, B., Nusbaum, C., Zody, M.C., Baldwin, J., Devon, K., Dewar, K., Doyle, M., FitzHugh, W., et al.; International Human Genome Sequencing Consortium (2001). Initial sequencing and analysis of the human genome. Nature *409*, 860–921.

Lehnertz, B., Ueda, Y., Derijck, A.A., Braunschweig, U., Perez-Burgos, L., Kubicek, S., Chen, T., Li, E., Jenuwein, T., and Peters, A.H. (2003). Suv39h-mediated histone H3 lysine 9 methylation directs DNA methylation to major satellite repeats at pericentric heterochromatin. Curr. Biol. *13*, 1192–1200.

Li, Z., Cao, R., Wang, M., Myers, M.P., Zhang, Y., and Xu, R.M. (2006). Structure of a Bmi-1-Ring1B polycomb group ubiquitin ligase complex. J. Biol. Chem. *281*, 20643–20649.

Long, H.K., Blackledge, N.P., and Klose, R.J. (2013a). ZF-CxxC domain-containing proteins, CpG islands and the chromatin connection. Biochem. Soc. Trans. *41*, 727–740.

Long, H.K., Sims, D., Heger, A., Blackledge, N.P., Kutter, C., Wright, M.L., Grützner, F., Odom, D.T., Patient, R., Ponting, C.P., and Klose, R.J. (2013b). Epigenetic conservation at gene regulatory elements revealed by non-methylated DNA profiling in seven vertebrates. Elife *2*, e00348.

Lynch, M.D., Smith, A.J., De Gobbi, M., Flenley, M., Hughes, J.R., Vernimmen, D., Ayyub, H., Sharpe, J.A., Sloane-Stanley, J.A., Sutherland, L., et al. (2012). An interspecies analysis reveals a key role for unmethylated CpG dinucleotides in vertebrate Polycomb complex recruitment. EMBO J. *31*, 317–329.

Marks, H., Kalkan, T., Menafra, R., Denissov, S., Jones, K., Hofemeister, H., Nichols, J., Kranz, A., Stewart, A.F., Smith, A., and Stunnenberg, H.G. (2012). The transcriptional and epigenomic foundations of ground state pluripotency. Cell *149*, 590–604.

Mayer, W., Niveleau, A., Walter, J., Fundele, R., and Haaf, T. (2000). Demethylation of the zygotic paternal genome. Nature *403*, 501–502.

Mendenhall, E.M., Koche, R.P., Truong, T., Zhou, V.W., Issac, B., Chi, A.S., Ku, M., and Bernstein, B.E. (2010). GC-rich sequence elements recruit PRC2 in mammalian ES cells. PLoS Genet. *6*, e1001244.

Meshorer, E., Yellajoshula, D., George, E., Scambler, P.J., Brown, D.T., and Misteli, T. (2006). Hyperdynamic plasticity of chromatin proteins in pluripotent embryonic stem cells. Dev. Cell *10*, 105–116.

Mohd-Sarip, A., Cléard, F., Mishra, R.K., Karch, F., and Verrijzer, C.P. (2005). Synergistic recognition of an epigenetic DNA element by Pleiohomeotic and a Polycomb core complex. Genes Dev. *19*, 1755–1760.

Ng, H.H., Jeppesen, P., and Bird, A. (2000). Active repression of methylated genes by the chromosomal protein MBD1. Mol. Cell. Biol. *20*, 1394–1406.

Oswald, J., Engemann, S., Lane, N., Mayer, W., Olek, A., Fundele, R., Dean, W., Reik, W., and Walter, J. (2000). Active demethylation of the paternal genome in the mouse zygote. Curr. Biol. *10*, 475–478.

Pengelly, A.R., Copur, O., Jäckle, H., Herzig, A., and Müller, J. (2013). A histone mutant reproduces the phenotype caused by loss of histone-modifying factor Polycomb. Science *339*, 698–699.

Peters, A.H., O'Carroll, D., Scherthan, H., Mechtler, K., Sauer, S., Schöfer, C., Weipoltshammer, K., Pagani, M., Lachner, M., Kohlmaier, A., et al. (2001). Loss of the Suv39h histone methyltransferases impairs mammalian heterochromatin and genome stability. Cell *107*, 323–337.

Peters, A.H., Kubicek, S., Mechtler, K., O'Sullivan, R.J., Derijck, A.A., Perez-Burgos, L., Kohlmaier, A., Opravil, S., Tachibana, M., Shinkai, Y., et al. (2003). Partitioning and plasticity of repressive histone methylation states in mammalian chromatin. Mol. Cell *12*, 1577–1589.

Plath, K., Fang, J., Mlynarczyk-Evans, S.K., Cao, R., Worringer, K.A., Wang, H., de la Cruz, C.C., Otte, A.P., Panning, B., and Zhang, Y. (2003). Role of histone H3 lysine 27 methylation in X inactivation. Science *300*, 131–135.

Probst, A.V., and Almouzni, G. (2011). Heterochromatin establishment in the context of genome-wide epigenetic reprogramming. Trends Genet. *27*, 177–185.

Puschendorf, M., Terranova, R., Boutsma, E., Mao, X., Isono, K., Brykczynska, U., Kolb, C., Otte, A.P., Koseki, H., Orkin, S.H., et al. (2008). PRC1 and Suv39h specify parental asymmetry at constitutive heterochromatin in early mouse embryos. Nat. Genet. *40*, 411–420.

Reddington, J.P., Perricone, S.M., Nestor, C.E., Reichmann, J., Youngson, N.A., Suzuki, M., Reinhardt, D., Dunican, D.S., Prendergast, J.G., Mjoseng, H., et al. (2013). Redistribution of H3K27me3 upon DNA hypomethylation results in de-repression of Polycomb target genes. Genome Biol. *14*, R25.

Reik, W., Dean, W., and Walter, J. (2001). Epigenetic reprogramming in mammalian development. Science *293*, 1089–1093.

Richly, H., Rocha-Viegas, L., Ribeiro, J.D., Demajo, S., Gundem, G., Lopez-Bigas, N., Nakagawa, T., Rospert, S., Ito, T., and Di Croce, L. (2010). Transcriptional activation of polycomb-repressed genes by ZRF1. Nature *468*, 1124–1128.

Ringrose, L., and Paro, R. (2004). Epigenetic regulation of cellular memory by the Polycomb and Trithorax group proteins. Annu. Rev. Genet. *38*, 413–443.

Santos, F., Peters, A.H., Otte, A.P., Reik, W., and Dean, W. (2005). Dynamic chromatin modifications characterise the first cell cycle in mouse embryos. Dev. Biol. *280*, 225–236.

Schermelleh, L., Heintzmann, R., and Leonhardt, H. (2010). A guide to super-resolution fluorescence microscopy. J. Cell Biol. *190*, 165–175.

Schmiedeberg, L., Skene, P., Deaton, A., and Bird, A. (2009). A temporal threshold for formaldehyde crosslinking and fixation. PLoS ONE *4*, e4636.

Schmitges, F.W., Prusty, A.B., Faty, M., Stützer, A., Lingaraju, G.M., Aiwazian, J., Sack, R., Hess, D., Li, L., Zhou, S., et al. (2011). Histone methylation by PRC2 is inhibited by active chromatin marks. Mol. Cell *42*, 330–341.

Schoeftner, S., Sengupta, A.K., Kubicek, S., Mechtler, K., Spahn, L., Koseki, H., Jenuwein, T., and Wutz, A. (2006). Recruitment of PRC1 function at the initiation of X inactivation independent of PRC2 and silencing. EMBO J. *25*, 3110–3122.

Sharif, J., Muto, M., Takebayashi, S., Suetake, I., Iwamatsu, A., Endo, T.A., Shinga, J., Mizutani-Koseki, Y., Toyoda, T., Okamura, K., et al. (2007). The SRA protein Np95 mediates epigenetic inheritance by recruiting Dnmt1 to methylated DNA. Nature *450*, 908–912.

Silva, J., Mak, W., Zvetkova, I., Appanah, R., Nesterova, T.B., Webster, Z., Peters, A.H., Jenuwein, T., Otte, A.P., and Brockdorff, N. (2003). Establishment of histone h3 methylation on the inactive X chromosome requires transient recruitment of Eed-Enx1 polycomb group complexes. Dev. Cell *4*, 481–495.

Simon, J.A., and Kingston, R.E. (2013). Occupying chromatin: Polycomb mechanisms for getting to genomic targets, stopping transcriptional traffic, and staying put. Mol. Cell *49*, 808–824.

Tavares, L., Dimitrova, E., Oxley, D., Webster, J., Poot, R., Demmers, J., Bezstarosti, K., Taylor, S., Ura, H., Koide, H., et al. (2012). RYBP-PRC1 complexes mediate H2A ubiquitylation at polycomb target sites independently of PRC2 and H3K27me3. Cell *148*, 664–678.

Tsumura, A., Hayakawa, T., Kumaki, Y., Takebayashi, S., Sakaue, M., Matsuoka, C., Shimotohno, K., Ishikawa, F., Li, E., Ueda, H.R., et al. (2006). Maintenance of self-renewal ability of mouse embryonic stem cells in the absence of DNA methyltransferases Dnmt1, Dnmt3a and Dnmt3b. Genes Cells *11*, 805–814.

Varley, K.E., Gertz, J., Bowling, K.M., Parker, S.L., Reddy, T.E., Pauli-Behn, F., Cross, M.K., Williams, B.A., Stamatoyannopoulos, J.A., Crawford, G.E., et al. (2013). Dynamic DNA methylation across diverse human cell lines and tissues. Genome Res. *23*, 555–567.

Wang, L., Brown, J.L., Cao, R., Zhang, Y., Kassis, J.A., and Jones, R.S. (2004). Hierarchical recruitment of polycomb group silencing complexes. Mol. Cell *14*, 637–646.

Weinhofer, I., Hehenberger, E., Roszak, P., Hennig, L., and Köhler, C. (2010). H3K27me3 profiling of the endosperm implies exclusion of polycomb group protein targeting by DNA methylation. PLoS Genet. *6*, 6.

Whitcomb, S.J., Fierz, B., McGinty, R.K., Holt, M., Ito, T., Muir, T.W., and Allis, C.D. (2012). Histone monoubiquitylation position determines specificity and direction of enzymatic cross-talk with histone methyltransferases Dot1L and PRC2. J. Biol. Chem. *287*, 23718–23725.

Woo, C.J., Kharchenko, P.V., Daheron, L., Park, P.J., and Kingston, R.E. (2010). A region of the human HOXD cluster that confers polycomb-group responsiveness. Cell *140*, 99–110.

Woo, C.J., Kharchenko, P.V., Daheron, L., Park, P.J., and Kingston, R.E. (2013). Variable requirements for DNA-binding proteins at polycomb-dependent repressive regions in human HOX clusters. Mol. Cell. Biol. *33*, 3274–3285.

Wu, H., Coskun, V., Tao, J., Xie, W., Ge, W., Yoshikawa, K., Li, E., Zhang, Y., and Sun, Y.E. (2010). Dnmt3a-dependent nonpromoter DNA methylation facilitates transcription of neurogenic genes. Science *329*, 444–448.

Wu, X., Johansen, J.V., and Helin, K. (2013). Fbxl10/Kdm2b recruits polycomb repressive complex 1 to CpG islands and regulates H2A ubiquitylation. Mol. Cell *49*, 1134–1146.

Yuan, W., Xu, M., Huang, C., Liu, N., Chen, S., and Zhu, B. (2011). H3K36 methylation antagonizes PRC2-mediated H3K27 methylation. J. Biol. Chem. *286*, 7983–7989.

Yuan, W., Wu, T., Fu, H., Dai, C., Wu, H., Liu, N., Li, X., Xu, M., Zhang, Z., Niu, T., et al. (2012). Dense chromatin activates Polycomb repressive complex 2 to regulate H3 lysine 27 methylation. Science *337*, 971–975.

Cell Reports, Volume *7*

Supplemental Information

Targeting Polycomb to Pericentric Heterochromatin in Embryonic Stem Cells Reveals a Role for H2AK119u1 in PRC2 Recruitment

Sarah Cooper, Martin Dienstbier, Raihann Hassan, Lothar Schermelleh, Jafar Sharif, Neil P. Blackledge, Valeria De Marco, Sarah Elderkin, Haruhiko Koseki, Robert Klose, Andreas Heger, and Neil Brockdorff

Figure S1

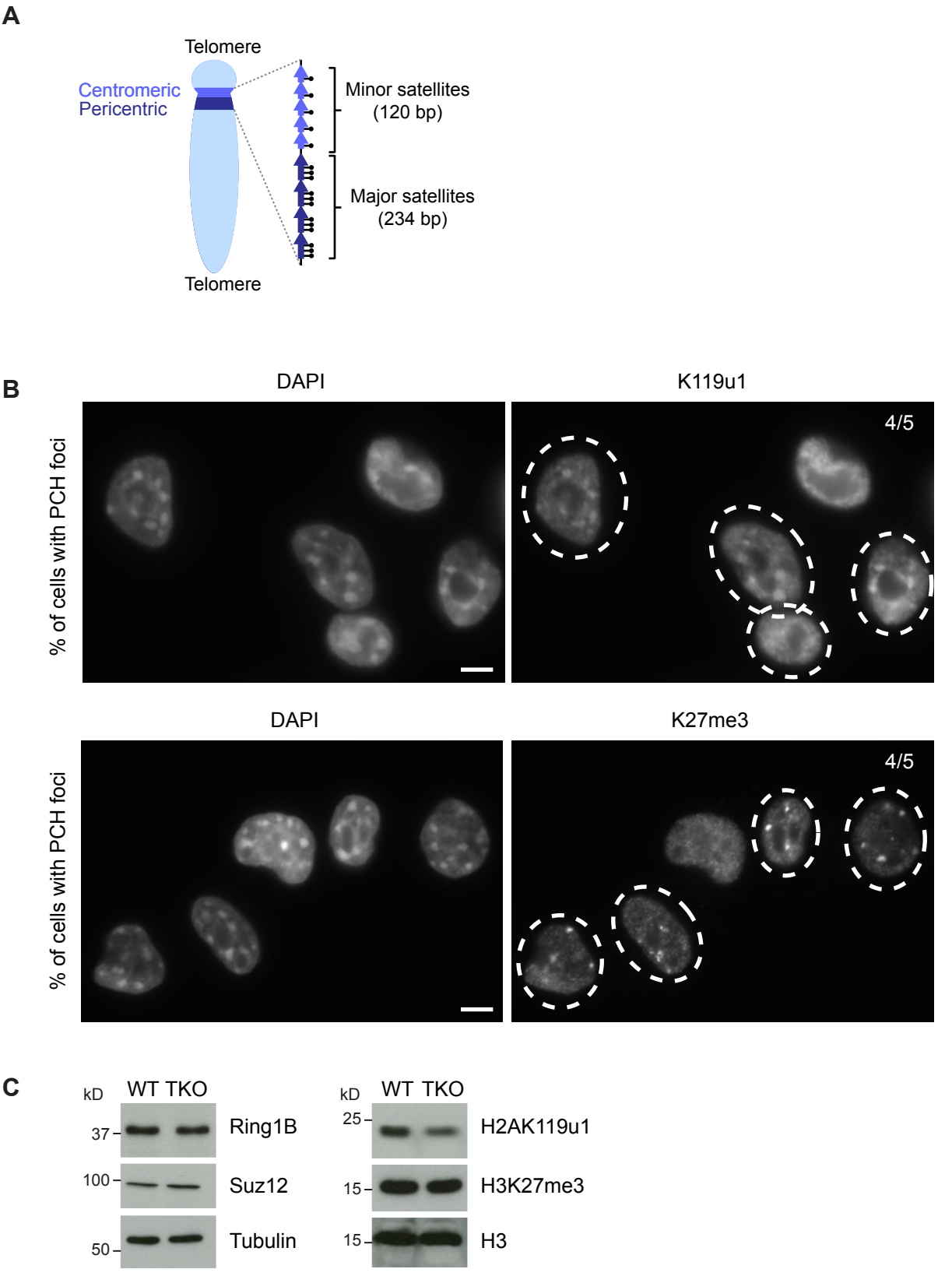
A
Telomere
Centromeric
Pericentric
Minor satellites
(120 bp)
Major satellites
(234 bp)
Telomere
B
DAPI
K119u1
4/5
% of cells with PCH foci
DAPI
K27me3
4/5
% of cells with PCH foci
C
kD
WT TKO
37
Ring1B
100
Suz12
50
Tubulin
kD
WT TKO
25
H2AK119u1
15
H3K27me3
15
H3

Figure S2

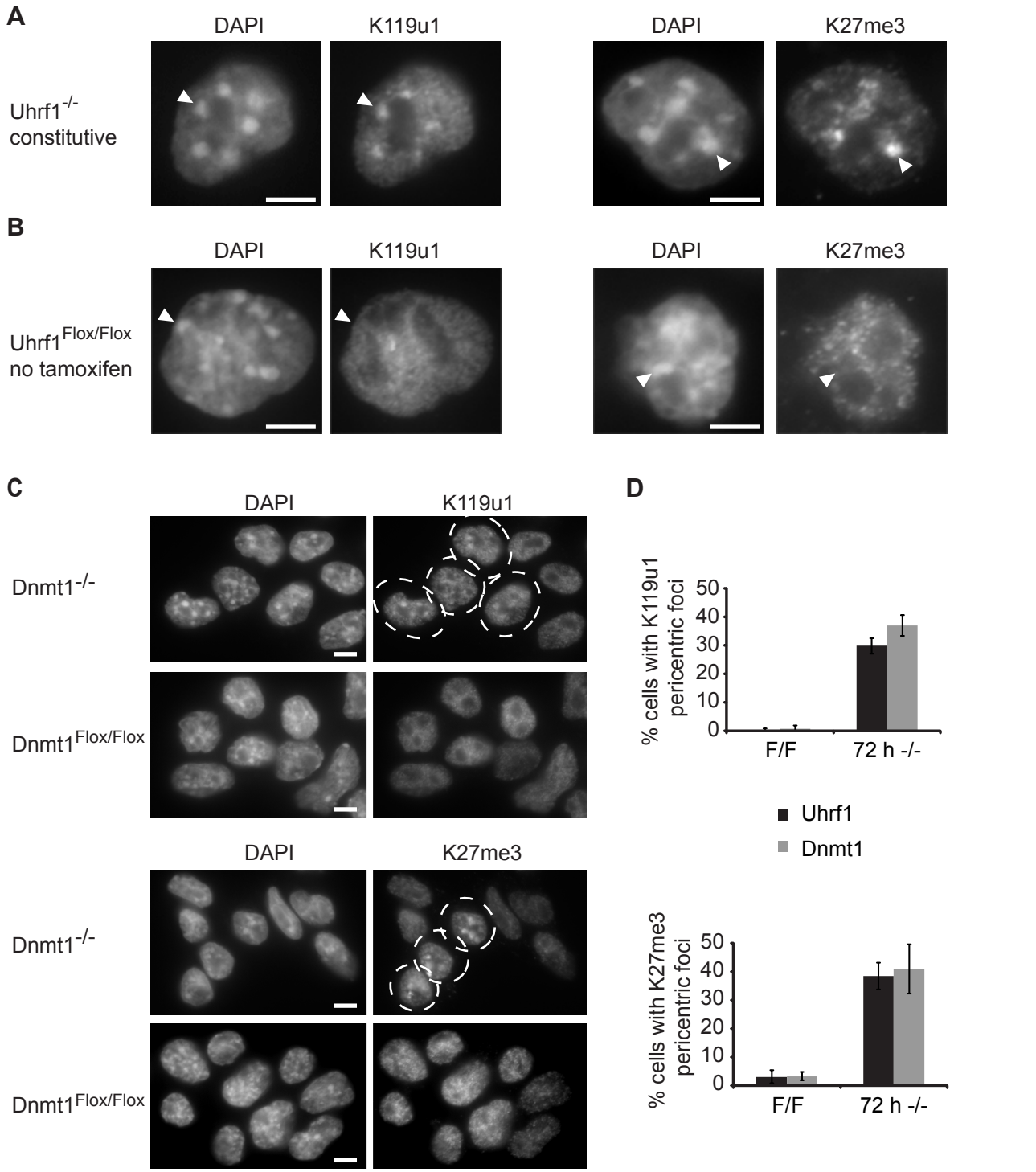
A
DAPI
K119u1
DAPI
K27me3
Uhrf1-/-
constitutive
B
DAPI
K119u1
DAPI
K27me3
Uhrf1Flox/Flox
no tamoxifen
C
DAPI
K119u1
Dnmt1-/-
Dnmt1Flox/Flox
DAPI
K27me3
Dnmt1-/-
Dnmt1Flox/Flox
D
% cells with K119u1 pericentric foci
50
40
30
20
10
0
F/F
72 h -/-
Uhrf1
Dnmt1
% cells with K27me3 pericentric foci
50
40
30
20
10
0
F/F
72 h -/-

Figure S3

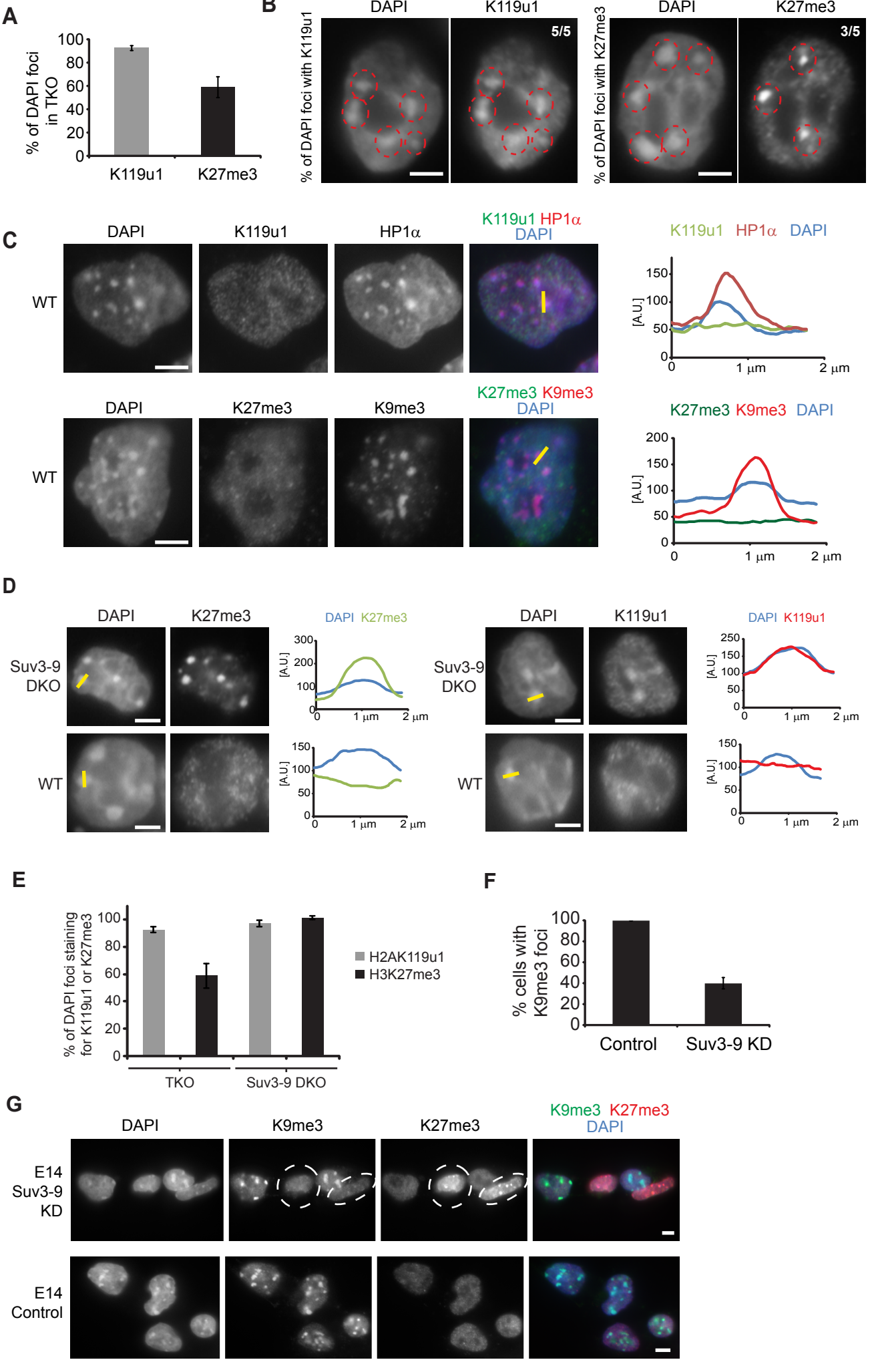
A
% of DAPI foci in TKO
100
80
60
40
20
0
K119u1
K27me3
B
DAPI
K119u1
% of DAPI foci with K119u1
5/5
DAPI
K27me3
% of DAPI foci with K27me3
3/5
C
DAPI
K119u1
HP1α
K119u1 HP1α DAPI
WT
K119u1 HP1α DAPI
[A.U.]
150
100
50
0
0
1 μm
2 μm
DAPI
K27me3
K9me3
K27me3 K9me3 DAPI
WT
K27me3 K9me3 DAPI
[A.U.]
200
150
100
50
0
0
1 μm
2 μm
D
DAPI
K27me3
DAPI K27me3
Suv3-9 DKO
WT
[A.U.]
300
200
100
0
150
100
50
0
0
1 μm
2 μm
DAPI
K119u1
DAPI K119u1
Suv3-9 DKO
WT
[A.U.]
250
150
100
50
0
150
100
50
0
0
1 μm
2 μm
E
% of DAPI foci staining for K119u1 or K27me3
100
80
60
40
20
0
H2AK119u1
H3K27me3
TKO
Suv3-9 DKO
F
% cells with K9me3 foci
100
80
60
40
20
0
Control
Suv3-9 KD
G
DAPI
K9me3
K27me3
K9me3 K27me3 DAPI
E14 Suv3-9 KD
E14 Control

Figure S4

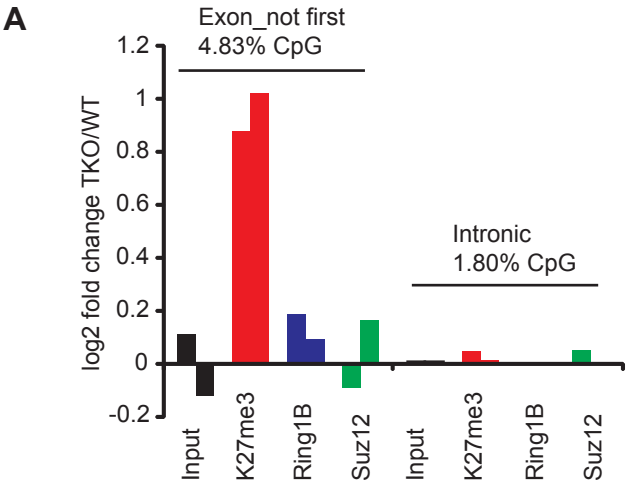
A
Exon_not first
4.83% CpG
Intronic
1.80% CpG
log2 fold change TKO/WT
1.2
1
0.8
0.6
0.4
0.2
0
-0.2
Input
K27me3
Ring1B
Suz12
Input
K27me3
Ring1B
Suz12

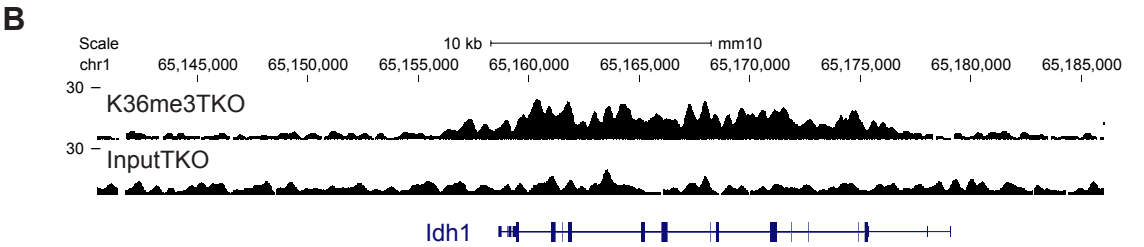
B
Scale
chr1
10 kb
mm10
65,145,000
65,150,000
65,155,000
65,160,000
65,165,000
65,170,000
65,175,000
65,180,000
65,185,000
30
K36me3TKO
30
InputTKO
Idh1

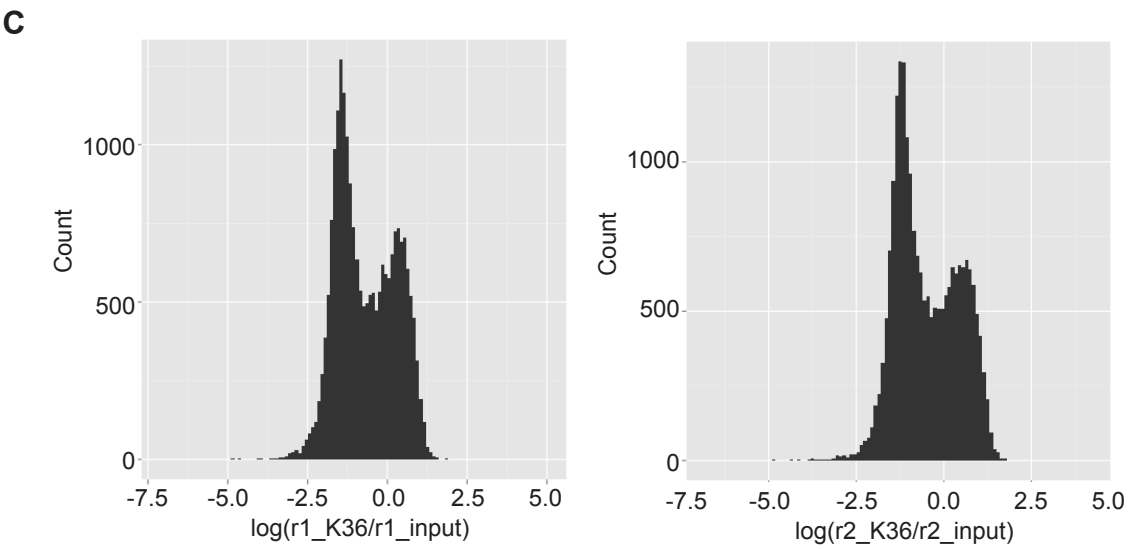
C
Count
1000
500
0
-7.5
-5.0
-2.5
0.0
2.5
5.0
log(r1_K36/r1_input)
Count
1000
500
0
-7.5
-5.0
-2.5
0.0
2.5
5.0
log(r2_K36/r2_input)

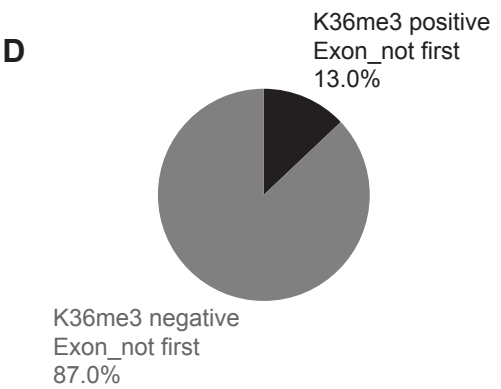
D
K36me3 positive
Exon_not first
13.0%
K36me3 negative
Exon_not first
87.0%

Figure S5

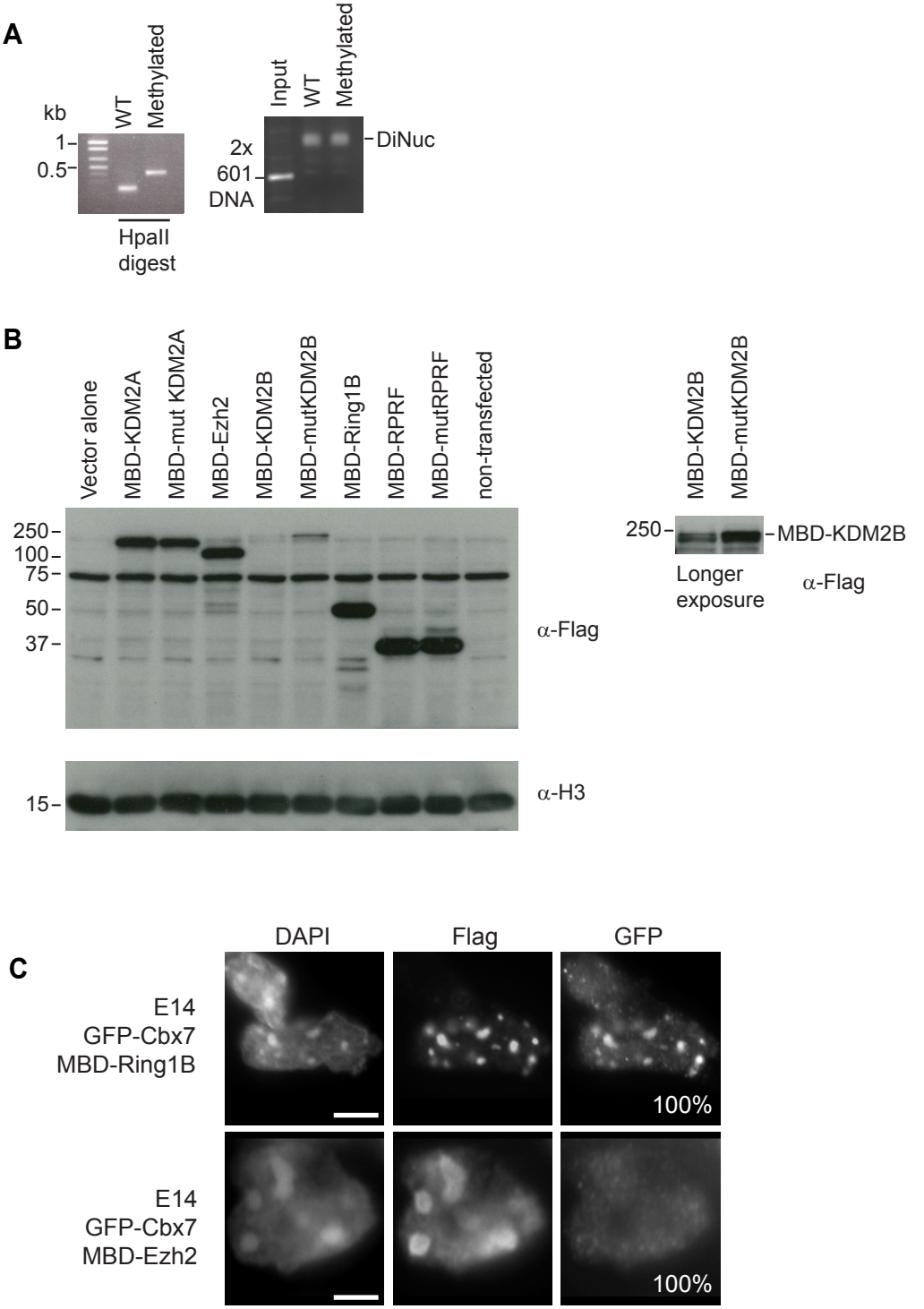
A
kb
WT
Methylated
1
0.5
HpaII digest
Input
WT
Methylated
2x 601 DNA
DiNuc
B
Vector alone
MBD-KDM2A
MBD-mut KDM2A
MBD-Ezh2
MBD-KDM2B
MBD-mutKDM2B
MBD-Ring1B
MBD-RPRF
MBD-mutRPRF
non-transfected
250
100
75
50
37
α-Flag
15
α-H3
MBD-KDM2B
MBD-mutKDM2B
250
MBD-KDM2B
Longer exposure
α-Flag
C
DAPI
Flag
GFP
E14
GFP-Cbx7
MBD-Ring1B
100%
E14
GFP-Cbx7
MBD-Ezh2
100%

Figure S6

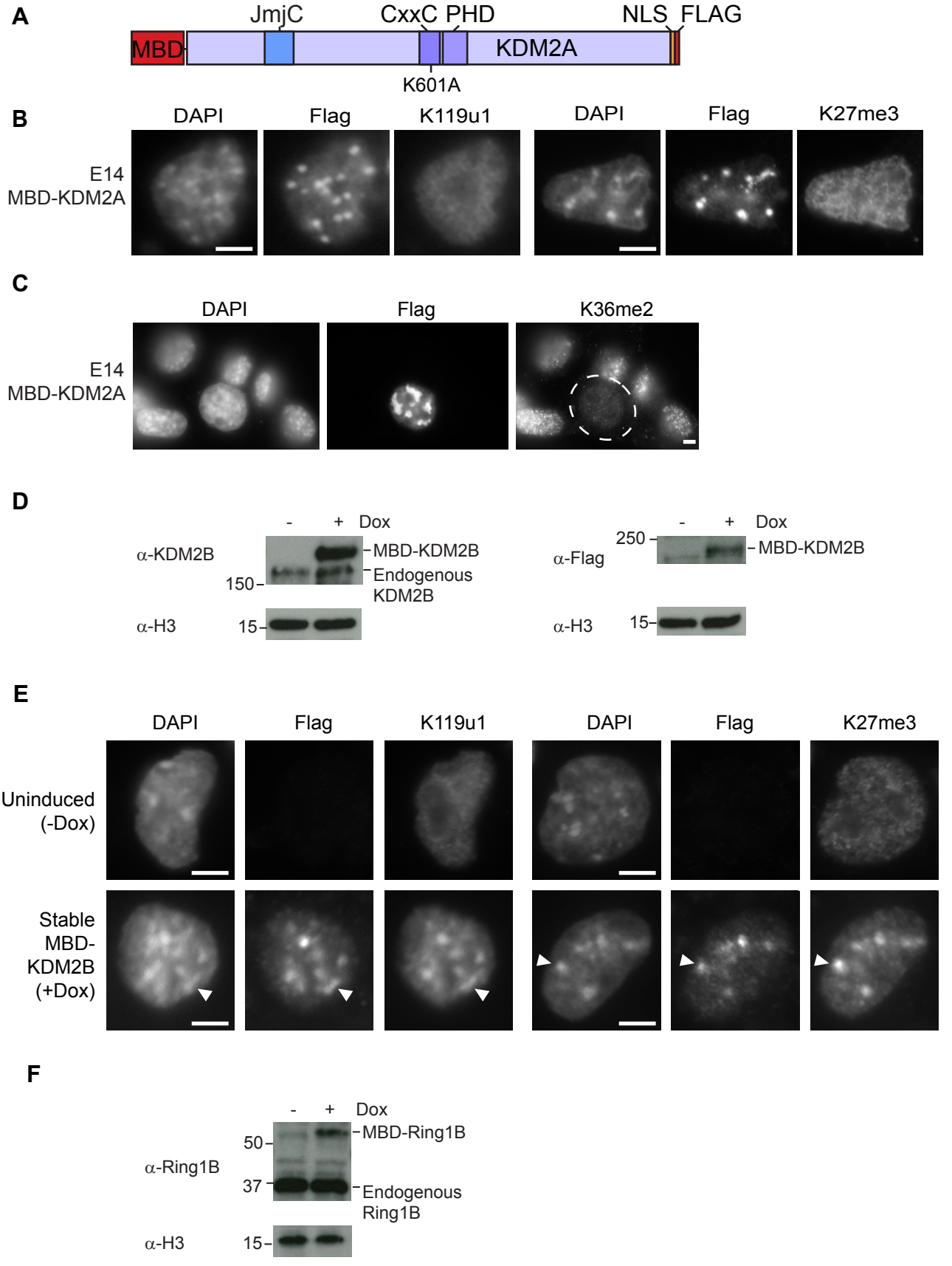
A
JmjC
CxxC PHD
NLS FLAG
MBD
KDM2A
K601A
B
DAPI
Flag
K119u1
DAPI
Flag
K27me3
E14
MBD-KDM2A
C
DAPI
Flag
K36me2
E14
MBD-KDM2A
D
- + Dox
α-KDM2B
MBD-KDM2B
150
Endogenous
KDM2B
α-H3
15
- + Dox
250
α-Flag
MBD-KDM2B
α-H3
15
E
DAPI
Flag
K119u1
DAPI
Flag
K27me3
Uninduced
(-Dox)
Stable
MBD-
KDM2B
(+Dox)
F
- + Dox
50
α-Ring1B
MBD-Ring1B
37
Endogenous
Ring1B
α-H3
15

Figure S7

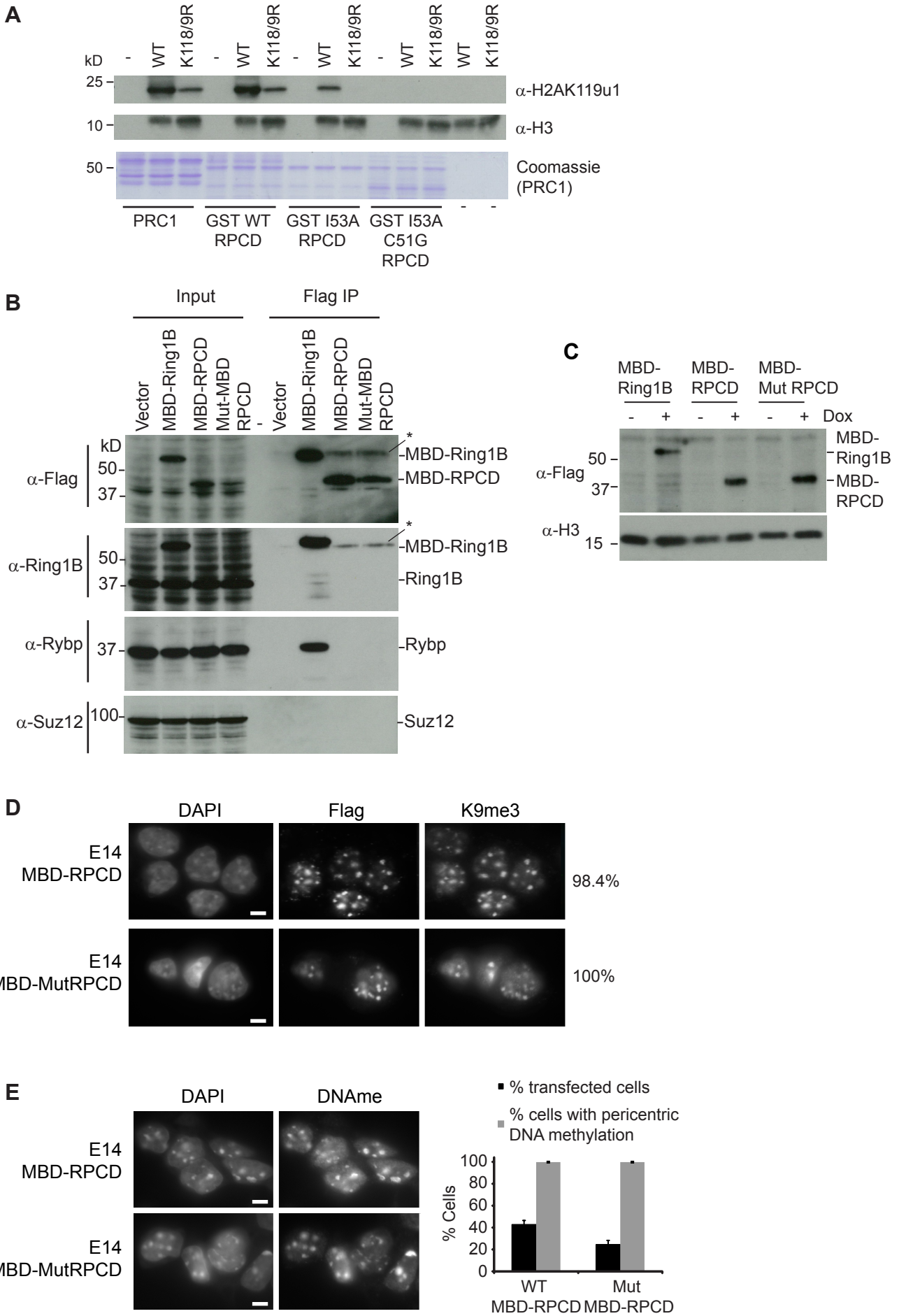
A
kD
-
WT
K118/9R
25
10
50
α-H2AK119u1
α-H3
Coomassie (PRC1)
PRC1
GST WT RPCD
GST I53A RPCD
GST I53A C51G RPCD
B
Input
Flag IP
Vector
MBD-Ring1B
MBD-RPCD
Mut-MBD RPCD
α-Flag
α-Ring1B
α-Rybp
α-Suz12
100
MBD-Ring1B
MBD-RPCD
Ring1B
Rybp
Suz12
C
MBD-Ring1B
MBD-RPCD
MBD-Mut RPCD
Dox
α-H3
15
D
DAPI
Flag
K9me3
E14 MBD-RPCD
E14 MBD-MutRPCD
98.4%
100%
E
DAPI
DNAme
% transfected cells
% cells with pericentric DNA methylation
% Cells
WT MBD-RPCD
Mut MBD-RPCD

Supplemental Figure Legends

Figure S1

PcG complexes localise to PCH in response to loss of DNA methylation. Related to Figure 1. A. Schematic of mouse PCH. B. IF of TKO cells stained for H2AK119u1 or H3K27me3, and DNA stained with DAPI, showing a typical field of view. Cells showing PCH foci positive for H2AK119u1 or H3K27me3 are circled in white to illustrate the scoring in Figure 1B. C. Western blot analysis of levels of PRC1 (Ring1B, H2AK119u1) and PRC2 (Suz12, H3K27me3) proteins and modifications, along with loading controls (Tubulin, histone H3), in WT and TKO cells. Scale bars 5 μm.

Figure S2

PcG complexes are dynamically acquired at PCH upon loss of DNA methylation. Related to Figure 2. A. IF of constitutive Uhrf1 $^{-/-}$ cells stained for H2AK119u1 or H3K27me3. Arrowheads indicate a single PCH domain. B. IF of WT (Uhrf $^{Flox/Flox}$) cells stained for H2AK119u1 or H3K27me3. Arrowheads indicate a single PCH domain. C. IF of Dnmt1 $^{-/-}$ (72 h, tamoxifen treatment) or WT (Dnmt1$^{Flox/Flox}$) cells stained for H2AK119u1 or H3K27me3. Cells showing PCH foci positive for H2AK119u1 or H3K27me3 are circled in white. D. Graphs to compare % of cells with H2AK119u1 or H3K27me3 foci in Uhrf1$^{-/-}$ and Dnmt1 $^{-/-}$ cells (72 h, tamoxifen treatment). Bars show average (n >200 cells) +/- SD (n=3). Scale bars 5 μm.

Figure S3

H3K9me3 antagonises PcG recruitment. Related to Figure 3. A. Graph to show % of DAPI foci staining for H2AK119u1 or H3K27me3 in TKO cells. Bars show average (n>200 DAPI foci) +/- SD (n=3). B. IF of TKO cells with DAPI foci, H2AK119u1 and H3K27me3 foci marked with red circles to illustrate scoring shown in A and Figure 3E. C. IF of WT cells co-stained for H2AK119u1 and HP1α, or H3K27me3 and H3K9me3. The graphs show a profile plot of fluorescence intensity (Arbitrary units, A.U.) across a single PCH domain (2 μM) defined by DAPI and marked on the merge image as a yellow bar. D. IF of Suv3-9h1/h2 DKO and WT cells stained for H3K27me3 (left) or H2AK119u1 (right). Graphs, as in C, show profiles of a single PCH domain marked as a yellow bar. E. Graph to show % of DAPI foci staining for H2AK119u1 (grey) or H3K27me3 (black) in TKO cells or in Suv3-9h1/h2 DKO cells. Bars show average (n>200 DAPI foci) +/- SD (n=3). F. Graph to show % cells with H3K9me3 foci in Uhrf1$^{-/-}$ cells upon Suv3-9h1/h2 knockdown. Bars show average (n >200 cells) +/- SD (n=3). G. Knockdown of Suv3-9h1/h2 or a scrambled control in E14

ESCs, co-stained for H3K27me3 and H3K9me3. White circles indicate cells with Suv3-9h1/h2 KD. Scale bars 5 µm.

Figure S4

Upon DNA methylation loss, PcG complexes are redistributed to exon sequences, defined by H3K36me3 occupancy. Related to Figure 4. A. Graph to show the fold change of reads, normalised to total reads, from ChIP-seq analysis of Input, H3K27me3, Ring1B and Suz12 in TKO relative to WT cells, at exons (excluding first exon) or introns. B. Screen shot of one biological repeat of ChIP-seq of H3K36me3 and Input in TKO cells. C. Distribution of fold change between H3K36me3 total read count and input total read count in two biological replicates. D. Pie chart to show % of exons (excluding first) which are defined as positive or negative for H3K36me3.

Figure S5. DNA methylation does not directly inhibit PcG activity in vitro or in vivo. Related to Figure 5 and 6. A. Left panel shows an agarose gel of a methylation sensitive digest (HpaII) of WT or in vitro methylated 601 positioning sequence DNA. Right panel shows EMSA analysis of reconstituted di-nucleosomes run on 0.8% agarose gel, post-stained with ethidium bromide. B. Western blot analysis, probed for Flag and H3, of whole cell extracts from E14 ESCs transiently transfected with MBD tethering constructs. Right panel shows longer exposure of same blot to highlight MBD-KDM2B constructs. C. MBD-Ring1B-Flag or MBD-Ezh2-Flag transfected into ESCs stably expressing GFP-Cbx7, stained for Flag and GFP. % of cells showing illustrated phenotype is indicated (n>100). Scale bars 5 µm.

Figure S6. KDM2B, but not KDM2A, can recruit PRC2 activity to PCH domains. Related to Figure 6. A. Schematic of MBD-KDM2A-Flag showing the position of the mutation in the CxxC domain (K-A). B. MBD-KDM2A-Flag transfected into E14 ESCs stained for H3K27me3 and H2AK119u1. C. As B, stained for Flag and H3K36me2. The white circle indicates reduction of H3K36me2 upon MBD-KDM2A expression. D. Western blot showing nuclear extracts from inducible stable MBD-KDM2B-Flag cell lines, plus or minus doxycycline, probed using an antibody against KDM2B (left) or Flag (right), and an antibody against histone H3 as a loading control. E. Inducible stable line expressing MBD-KDM2B-Flag, either non-induced or induced for 3 days with doxycycline, and stained for Flag and H2AK119u1 (left) and Flag and H3K27me3 (right). Arrowheads indicate an example of staining within Flag domains at PCH. F. Western blot showing whole cell

extracts from inducible stable MBD-Ring1B-Flag cell lines, plus or minus doxycycline, probed using an antibody against Ring1B and H3 (loading control). Scale bars 5 μm.

Figure S7. Ubiquitylated H2A is sufficient to recruit PRC2 to PCH domains. Related to Figure 7. A. PRC1 ubiquitylation assay using WT or H2AK118R/K119R nucleosomes as substrate, and analysed by western blot (probed for H2AK119u1 or H3). Recombinant PRC1 and RPCD proteins are shown by Coomassie staining (lower panel). B. Coimmunoprecipitation experiment using E14 cells transfected with empty vector, MBD-Ring1B-Flag, MBD-RPCD-Flag, or MBD-mut-RPCD-Flag and immunoprecipitated with Flag beads. Western blot analysis of Input samples and IP samples, probed for Flag, Ring1B, Rybp or Suz12 antibodies. * indicates antibody heavy chain. C. Western blot showing whole cell extracts from inducible stable MBD-Ring1B-Flag, MBD-RPCD-Flag and MBD-mut-RPCD-Flag cell lines, plus or minus doxycycline, probed using an antibody against Flag and H3 (loading control). D. MBD-RPCD-Flag or MBD-mutRPCD-Flag transfected into E14 ESCs and stained for Flag and H3K9me3. Number of transfected cells with H3K9me3 PCH domains indicated (n>200). E. MBD-RPCD-Flag or MBD-mutRPCD-Flag transfected into E14 ESCs and stained with meC antibody (DNAme). Graph shows % of transfected cells (determined by Flag staining) and % of cells with meC PCH domains. Bars show average (n> 200 cells) +/- SD (n=3). Scale bars 5 μm.

Table S1

Excel table showing fold changes in TKO cells relative to WT cells at all classes of repeat. Related to Figure 4.

Table S2

Oligonucleotide sequences. Related to Figure 3 and 4.

Name	Sequence
Nkx2.25'UTRF	GTCGCTGACCAACACAAAGACG
Nkx2.25'UTRR	TGTCGTAGAAAGGGCTCTTAAGGG
Nkx2.23'UTRF	AAAGTATGCCAACTCGGTGCCA
Nkx2.23'UTRR	GGAAGATAATCTTCTGGGCTCCCA
Dlx1 F	ATGTCTCCTTCTCCCATGTCC
Dlx1 R	ACTGCACGGAACTGATGTAGG
NanogF	CCCAGGTTTCCCAATGTGAAG
NanogR	AAAGAGTCAGACCTTGCTGCCA
Map3k1F	GGGAGGGGACACCTACAGAT
Map3k1R	TTGGGCGCTTAGTGTTTTGC
Sh3bp4F	CGGGCACATCTTCCTTCACT
Sh3bp4R	ATCCGATTTGGCTTGCAGGA
Lrrc8cF	TCTGATTGTGCACTGGGCAT
Lrrc8cR	AGTGCTGTATCCATGGAGTGT
Auts2F	GTCTCTTCGGTGCATGTCCA
Auts2R	CAGGACACGTATGGTGACCC
Suv39H1F1	CCGGGCCTTTGTACTCAGGAAAGAACTCGAGTTCTTTCCTGAGTACAAAGGCTTTTTG
Suv39H1R1	AATTCAAAAAGCCTTTGTACTCAGGAAAGAACTCGAGTTCTTTCCTGAGTACAAAGGC
Suv39H1F2	CCGGCCTGCACAAGTTTGCCTACAACTCGAGTTGTAGGCAAACTTGTGCAGGTTTTTG
Suv39H1R2	AATTCAAAAACCTGCACAAGTTTGCCTACAACTCGAGTTGTAGGCAAACTTGTGCAGG
Suv39H2F1	CCGGCGGTAGATATTTGGTGGTTAACTCGAGTTAACCACCAAATATCTACCGTTTTTG
Suv39H2R1	AATTCAAAAACGGTAGATATTTGGTGGTTAACTCGAGTTAACCACCAAATATCTACCG
Suv39H2F2	CCGGCCACCTTTGGATGTTCATGTACTCGAGTACATGAACATCCAAAGGTGGTTTTTG
Suv39H2R2	AATTCAAAAACCACCTTTGGATGTTCATGTACTCGAGTACATGAACATCCAAAGGTGG

Table S3

Number of mapped reads from ChIP-seq samples. Related to Figure 4.

			Mapped pairs		Uniquely mapped pairs	
Track	**read length**	**total**	**pairs**	**percent**	**pairs**	**percent**
TKO-H3K27me3-R1.bwa	51	51,753,880	47,801,066	92%	38,230,376	74%
TKO-H3K27me3-R2.bwa	51	52,935,084	47,437,675	90%	37,591,517	71%
TKO-Input-R1.bwa	51	79,405,963	74,102,709	93%	59,330,219	75%
TKO-Input-R2.bwa	51	108,134,176	99,082,632	92%	78,858,197	73%
TKO-H3K36me3-R1.bwa	51	51,993,486	46,469,313	89%	36,924,092	71%
TKO-H3K36me3-R2.bwa	51	51,930,671	47,289,433	91%	37,410,446	72%
TKO-Ring1B-R1.bwa	51	98,659,073	89,163,267	90%	69,934,793	71%
TKO-Ring1B-R2.bwa	51	96,352,121	88,507,254	92%	70,592,334	73%
TKO-Suz12-R1.bwa	51	98,415,365	91,717,592	93%	75,501,142	77%
TKO-Suz12-R2.bwa	51	89,195,230	81,694,305	92%	65,136,943	73%
WT-H3K27me3-R1.bwa	51	46,490,832	43,251,087	93%	36,023,542	77%
WT-H3K27me3-R2.bwa	51	48,635,176	46,107,145	95%	38,687,931	80%
WT-Input-R1.bwa	51	123,066,448	114,053,963	93%	92,277,787	75%
WT-Input-R2.bwa	51	103,255,996	94,941,273	92%	75,021,400	73%
WT-H3K36me3-R1.bwa	51	48,065,277	43,436,203	90%	35,328,149	74%
WT-H3K36me3-R2.bwa	51	53,347,488	47,411,148	89%	39,150,307	73%
WT-Ring1B-R1.bwa	51	117,134,292	105,842,041	90%	85,555,833	73%
WT-Ring1B-R2.bwa	51	104,120,041	96,667,105	93%	78,390,261	75%
WT-Suz12-R1.bwa	51	119,071,917	110,575,020	93%	89,603,897	75%
WT-Suz12-R2.bwa	51	101,715,954	94,788,697	93%	77,113,448	76%

Extended Experimental Procedures

Cells

ESCs were grown in ES media (Dulbecco's Modified Eagle Medium (DMEM, Life Technologies) supplemented with 10% foetal calf serum (FCS, Seralab), 2 mM L-glutamine, 1x non-essential amino acids, 50 μM 2-mercaptoethanol, 50 μg/ml penicillin/streptomycin (Invitrogen) and LIF-conditioned medium, made in house, at a concentration equivalent to 1000 U/ml. Feederless ESCs were grown on tissue culture dishes coated with PBS+1% gelatine, and feeder-dependent ESCs were grown on mitomycin inactivated primary embryonic fibroblasts (PEFs). Mouse embryonic fibroblasts (MEFs) were grown in EC10 medium (DMEM, supplemented with 10% FCS, 2 mM L-glutamine, 1x non-essential amino acids, 50 μM 2-mercaptoethanol and 50 μg/ml penicillin/streptomycin).

The following cell lines were used in this study : E14TG2A, TKO ($Dnmt1^{-/-}$, $Dnmt3a^{-/-}$, $Dnmt3b^{-/-}$) and matched WT (J1) ESCs (Tsumura et al., 2006), 293 cells, conditional $Uhrf1^{-/-}$, $Dnmt1^{-/-}$ and matched WT (E14) ESCs (Sharif et al., 2007), Suv3-9h1/h2 DKO, and matched WT (E14) ESCs (Peters et al., 2003). Conditional Uhrf1 and Dnmt1 knockout cells were grown on inactivated PEFs and gene deletion was carried out by the addition of 800 nM 4-hydroxytamoxifen.

Stable clonal GFP-Cbx7 ESC lines were produced by transfecting GFP-Cbx7 in pCAG-IP (gift from Ian Chambers) into 129/1 feeder dependent ESCs and puromycin selection. Inducible, stable, clonal MBD-KDM2B, MBD-Ring1B, MBD-RPCD and MBD-mutRPCD lines were produced by co-transfecting MBD-fusions in pTRE-Tight (Clontech, see below) and pNeo Bluescript (that expresses neomycin resistance gene under the constitutive PGK promoter), into rtTA2A10 ESC lines (in which the rtTA gene is integrated into the Rosa26 locus, targeting construct gift from Anton Wutz) and selecting with G418. MBD-fusion protein expression was induced by addition of 1 μg/ml doxycycline for 3 days. WT MEFs, $Dnmt1^{-/-}$, $p53^{-/-}$ MEFs and matched control ($p53^{-/-}$) MEFs (Lande-Diner et al., 2007) were grown in EC10 medium. MEFs from $Dnmt1^{-/-}$, $p53^{+/+}$ embryos were unable to be cultured, suggesting that, unlike in ESCs, p53 is essential to protect MEFs from demethylation (Lande-Diner et al., 2007).

Constructs

Amino acids 1-112 of human MBD1, which include the MBD domain and endogenous NLS signal, followed by a glycine, serine rich flexible linker, were cloned to the N-terminus of the protein of interest in pBluescript. A SV40 NLS, followed by a FLAG-tag were cloned on the C-terminus of the protein of interest. These MBD-fusion proteins were then cloned into the mammalian expression plasmid pCAG, in which the MBD-fusion protein was under the control of the constitutive β-actin promoter. Full length mouse Ezh2, mouse Ring1B, and human KDM2A (K601A) and KDM2B (K643A) were targeted to methylated DNA using the MBD domain. For KDM2A/B the CxxC DNA binding domains were mutated (K601A and K643A respectively). The MBD-KDM2B, MBD-Ring1B, MBD-RPCD and MBD-mutRPCD constructs were also cloned into the pTight vector to allow doxycyline inducible expression when stably integrated into rtTA2A10 ESCs (see above).

Amino acids 1-116 of Ring1B and 3-109 of Pcgf4 (termed Ring1b Pcgf4 catalytic domain RPCD fusion) were joined using a 4x GGS flexible linker and cloned with an N-terminal GST tag in pGex-6p2 for bacterial protein expression and purification, or with an N terminal MBD domain in the pCAG vector, for expression in ESCs. Catalytic mutants were made in the JmjC domain of KDM2B (H242A, I243A, D244A), and in RPCD at Ring1B I53A to mutate the E2 interaction domain and at Pcgf4 C51G to mutate the zinc finger domain, using site-directed mutagenesis kit (Stratagene). Synthesised core PRC2 subunits (full length EZH2, EED, SUZ12 and RbAp48) were codon optimized for expression in insect cells (GeneArt) and cloned into pBAC4x-1 (Novagen) using In-fusion cloning (Clontech).

Immunofluorescence

ESCs or MEFs were split onto slides 16 h before staining at low density (without feeders). Slides were then washed in PBS, fixed with 2% formaldehyde in PBS for 15 min and permeablised with 0.4% Triton X-100 in PBS for 5 min. After washing with PBS, the slides were blocked for 30 min in 0.2% fish gelatin (Sigma) in PBS and incubated for 2 h with primary antibody (diluted in 0.2% fish gelatin, and 5% normal goat serum). Slides were washed 3 times in 0.2% fish gelatin and incubated for 2 h with Alexa-fluor conjugated secondary antibody (Life Technologies). After washing 2 times in fish gelatin, and 2 times in PBS, the slides were stained with DAPI (1 µg/ml), and mounted using mounting media (Dako).

The following primary antibodies were used for immunofluroscence : H2AK119u1 (1:500, Cell Signalling, rabbit monoclonal, 8240), H3K27me3 (1:500, Diagenode,rabbit polyclonal, pAB-069-050), H3K27me3 (1:1000, Active Motif, mouse monoclonal, 61017), Flag (1:500, Sigma M2, mouse monoclonal), H3K9me3 (1:500, Active motif, rabbit polyclonal 39161), H3K4me3 (1:500, Abcam, rabbit polyclonal, ab8580), HP1α (1:500, Millipore, mouse monoclonal MAB3584) and GFP (1:100, Santa Cruz, mouse monoclonal, sc-9996).

DNA methylation staining

Slides were fixed in 4% formaldehyde for 15 min, permeablised in 0.2% Triton X-100 for 1 h and washed in 0.05% Tween-200 in PBS 3 times. They were then treated with 4M HCl with 0.1% Triton X-100 for 10 min and neutralised with 100 mM Tris-HCl pH8.8 for 30 min. After blocking overnight in 1% BSA, 0.05% Tween-20 in PBS, the primary antibody (1:500 Eurogentec, mouse monoclonal, BI-MECY-0100) was added overnight in blocking solution. Slides were washed extensively in blocking solution, secondary antibody was added for 2 h, and slides were washed again in blocking buffer and PBS before mounting (as above).

Cell transfection

ESCs or T16 MEFs were plated in a 6 well dish 16 h before transfection in ES or EC10 media without pen/strep. One hour before transfection, the media was changed. DNA (4 µg) was mixed with 8 µl lipofectamine in Optimem media, and incubated for 20 min before adding to cells. The media was changed 6 h later, and 16 h the cells were split to a 90 mm dish. The cells were split the next day to slides and fixed for immunofluorescence the following day (3 days after the initial transfection).

Quantification of PCH staining phenotypes

Slides were visualised using a 63x oil immersion objective with the Zeiss Axio Observer Z1 microscope.

Unbiased quantification of PCH enrichment

After applying a Gaussian blur filter to the images, the total nuclear area and PCH domains were defined using the Image J threshold algorithm, Triangle, based on the DAPI intensity (http://rsbweb.nih.gov/ij). The fluorescence intensity of H2AK119u1 or H3K27me3 staining

within PCH regions was then measured and expressed relative to the fluorescence intensity of the whole nucleus.

% of cells with PCH foci

The number of cells containing visible H2AK119u1 or H3K27me3 stained PCH were counted out of the total number of cells or total number of transfected cells (n>200), for three biological repeats. Error bars show standard deviation of biological repeats.

% DAPI foci

In cells with visible PCH foci, the number of foci positive for H3K27me3 or H2AK119u1 were counted out of the total number of DAPI foci (n>200), for three biological repeats. Error bars show standard deviation of biological repeats.

PCH domain cross-section analysis

A 2 µm line was drawn in Image J (shown by a yellow bar) across the PCH domain as determined by DAPI staining and the profile plot of fluorescence (arbitrary units) from each channel was obtained.

Super-resolution 3D-structured illumination microscopy (3D-SIM)

3D-SIM of immunostained ESC was performed on a DeltaVision OMX V3 Blaze system (Applied Precision Imaging/GE Healthcare), equipped with 60x/1.42 NA PlanApo oil immersion objective (Olympus), and 405, 488 and 592 nm diode lasers and Edge sCMOS cameras (PCO). SI image stacks were acquired with a z-distance of 125 nm and with 15 raw SI images per plane (5 phases, 3 angles). The SI raw data sets were computationally reconstructed with channel specific measured optical transfer functions (OTFs) and Wiener filter set to 0.003 using the softWoRX 6.0 software package (Applied Precision) to result in a 2-fold improvement of both lateral and axial resolution (Schermelleh et al., 2008). The refractive indices of the immersion oil for sample acquisition and measuring OTFs from 0.1 µm diameter FluoSphere beads (Invitrogen) were carefully selected to minimise spherical aberration. Images from the different colour channels were registered with alignment parameters obtained from calibration measurements with 0.2 µm diameter TetraSpeck beads (Invitrogen) using image registration with a linear fitting model implemented SoftWoRx 6.0. For display purposes the 32-bit reconstructed datasets were rescaled using the mode value as lower threshold for each channel to cut off half of the background and then converted to 16-bit composite tif-stacks using ImageJ.

Southern blot

Genomic DNA from conditional Uhrf1 cells was digested with the methylation sensitive enzyme HpyCH41V, separated on a 1.25% agarose gel and blotted to a hybond-XL membrane. Blots were probed with a 'gamma' mouse major satellite probe (Zvetkova et al., 2005) labelled using klenow and alpha-P-32-ATP.

Protein extract

Cells were harvested, washed in PBS and lysed with SDS-loading buffer before analysis by 12% SDS PAGE and western blot. Antibodies : Suz12 (1:250, Cell signalling, 3737S), Tubulin (1:250, Cell signalling, 2144) , Ring1B (1:1000, (Atsuta et al., 2001)) , H2AK119u1 (1:1000, Cell signalling, 8240), H3K27me3 (1:1000, Diagenode, pAB -069-100), H3 (1:10000, Abcam Ab1791) and Flag (1:1000, Sigma M2 HRP conjugated).

Chromatin Immunoprecipitation

ChIP from WT or TKO cells was performed as described in Blackledge et al., 2010 using the following antibodies : H3K27me3 (Diagenode pAB -069-100), H3K36me3 (Abcam AB9050), Suz12 (Cell Signalling 3737S), Ring1B (Atsuta et al., 2001) and H2AK119u1 (Cell signalling 8240). Three biological repeats were performed for qPCR analysis and two biological repeats were performed and, along with input samples, sent for high throughput sequencing.

Briefly, 5 x 10^7 cells were fixed with 2 µM Ethylene glycol bis[succinimidylsuccinate] (ThermoScientific) for 1 h and then 1% formaldehyde for 15 min at RT. The reaction was quenched with glycine (0.125M) and nuclei prepared in LB1 (50 mM HEPES-KOH, pH 7.9, 140 mM NaCl, 1 mM EDTA-NaOH pH 8.0, 10% Glycerol, 0.5% NP-40, 0.25% Triton X-100 and 1x complete EDTA-free protease inhibitors (Roche)). Nuclei were washed in LB2 (10 mM Tris-HCl, pH8.0, 200 mM NaCl, 1 mM EDTA-NaOH pH 8.0, 0.5 mM EGTA and 1x complete EDTA-free protease inhibitors) and lysed in LB3 (10 mM Tris-HCl, pH 8, 100 mM NaCl, 1 mM EDTA-NaOH pH 8.0, 0.5 mM EGTA, 0.1% Na-Deoxycholate, 0.5% *N*-lauroylsarcosine and 1x complete EDTA-free protease inhibitors). Chromatin was sheared in a BioRuptor sonicator (Diagenode) to produce DNA fragments with a length of <1 kb. Triton X-100 was added (1% final) and cell debris cleared by centrifugation before the sample was diluted ten-fold with dilution buffer (1% Triton X-100, 2 mM EDTA-NaOH pH 8.0, 150 mM NaCl, 20 mM Tris-HCl pH 8.0 and 1x complete EDTA-free protease inhibitors).

Samples were pre-cleared and incubated with antibodies overnight at 4°C, after removal of input aliquots. Antibody complexes were collected with 30 µl BSA and tRNA blocked rProtein A Sepharose beads and were washed once with low salt buffer (0.1% SDS, 1% Triton X-100, 2 mM EDTA-NaOH pH 8.0, 150 mM NaCl, 20 mM Tris-Cl pH 8.0), high salt buffer (0.1% SDS, 1% Triton-X-100, 2 mM EDTA-NaOH pH 8.0, 150 mM NaCl, 20 mM Tris-Cl pH 8.0), LiCl buffer (0.25 M LiCl, 1% NP-40, 1% Na-Deoxycholate, 1 mM EDTA-NaOH pH 8.0, 10 mM TrisHCl pH 8.0) and twice with TE buffer. Complexes were eluted from beads by incubation with 100 µl Elution Buffer (1% SDS, 0.1 M $NaHCO_3$) first at 65°C for 5 min, and subsequently for 30 min with vortexing at 25°C. NaCl was added to a final concentration of 200 mM and cross-links were reversed overnight at 65°C. DNA was recovered after treatment with 100 µg/ml DNase-free RNase A at 42°C for 90 min and Proteinase K (0.2 mg/ml) for 1 h at 45°C using ChIP DNA Clean & concentration columns (Zymo) and eluted in 10 µl volume. Samples for qPCR analysis were diluted 10-fold and analysed using a Biorad Chromo4 real time PCR machine (see Table S2 for primer sequences).

ChIP-seq

For ChIP-seq, undiluted purified DNA concentration was quantified using the PicoGreen dsDNA Quantitation Kit (Molecular Probes) and post-sonicated to <300 bp. Around 30 ng was sent to the Oxford Genomics Centre and 5 ng was used to prepare libraries using the NEBNext DNA Library Prep Master Mix Set for Illumina. Libraries were sequenced on an Illumina HiSeq2000 50bp paired end run.

Reads were mapped to the GRCm38 Mus musculus assembly from the UCSC genome browser (mm10, (Meyer et al., 2013) using bwa version 0.5.9-r16 (Li and Durbin, 2009) with the following options: “bwa aln -l 25 -k 2 -n 2”. BWA randomly selects a single position for reads mapping to multiple locations equally well. This mapping strategy permits quantification of the number of reads falling into different repeat categories. The number of pairs sequenced, mapped and mapped uniquely are in Table S3.

To test for local fold changes in read density, we used a window-based approach. Uniquely mapping read-pairs were counted by mid-point-overlap within 1kb windows tiled over the genome. Windows with more than 100 read pairs in input data were removed. Difference in fold change was tested using DESeq (Anders and Huber, 2010) pooling samples for dispersion estimates. We accepted windows with a 10% FDR.

Genomic annotations were obtained from the UCSC genome browser (repeats) and ENSEMBL version 72 ((Flicek et al., 2013) transcript models). We defined non-methylated

islands as the union of BioCAP-seq data from mouse testes, liver and ES cells obtained from (Long et al., 2013). Reads and genomic intervals were processed with bedtools (Quinlan and Hall, 2010). CpG content was calculated with in-house scripts.

Active and inactive genes in the TKO were defined through H3K36me3 data . Genes where both replicates contained more H3K36me3 than input reads across the genomic span were defined as active and vice versa for inactive genes (Cutoff 0 log fold change) (Figure S4).

Stable Suv3-9 H1 and H2 knockdown

Production of shRNA plasmids and lentivirus packaging were performed as previously described Tavares et al., 2012. Briefly, oligos (sequences in Table S2) were annealed and cloned into the pLK01 vector. This vector, along with packaging vectors were transfected into 293 cells using calcium phosphate transfection and 48 h later the supernatant was harvested containing lentivirus packaged shRHA hairpin.

ESCs (E14 or Uhrf1$^{-/-}$) (7.5× 10^5 per well of a 6-well dish) were plated with 250 µl of each lentivirus (Suv3-9h1 and Suv3-9h2) or scrambled control and polybrene (final concentration 8 µg/ml). Selection (1.75 µg/ml puromycin) was applied 48 hours after transduction. Cells were split to slides the day before fixing for immunofluorescence (day 6 after virus infection).

Histone purification and nucleosome reconstitution

Reconstitution of nucleosomes was performed as previously described. Briefly, recombinant Xenopus histones were expressed in bacteria and purified from inclusion bodies. H3K36CC110A mutant histone was also purified and chemically methylated in vitro (Simon, 2010). Stoichiometric amounts of each core histone were incubated together under high-salt conditions, and the resulting histone octamer was purified using a Superdex 200 gel filtration column (GE Healthcare). DNA containing two repeats of the nucleosome positioning sequence (601) and 48 bp linker was amplified by PCR and purified. DNA was then methylated using Sss1 (NEB) and methylation was assayed using methylation sensitive enzyme (HpaII) digest.

Equimolar ratios of DNA (WT or methylated) and octamers (WT or H3K36me3) were mixed together in 2 M NaCl and diluted stepwise with 10 mM Tris-HCl, pH 7.5, to reach a final concentration of 100 mM NaCl. The reconstituted dinucleosomes were analysed by an

electrophoretic mobility shift assay (EMSA) using 0.8% agarose gel in 0.2% Tris-borate and post stained with ethidium bromide.

PRC2 purification and HMTase Assay

PRC2 core complex (EZH2, EED, SUZ12 and RbAp48) in pBAC4x-1 was coexpressed using baculovirus and purified from SF9 cells. *Sf9* cells were cultured in SF900 II serum free media (Invitrogen) at 28°C. In a typical preparation, 1L of *Sf9* cells at $2x10^6$ cells/ml density was infected with 3ml of high titre PRC2 virus for 48 h. Cells were consequently harvested, washed in ice cold PBS, resuspended in potassium phosphate 20mM pH 8.0, KCl 100mM, Triton X 100 0.01%, TCEP 1mM and lysed in an EmulsiFlex-C5 homogenizer (Avestin). The complex was initially purified by affinity chromatography using the Strep(II) tag engineered at the N-terminus of EZH2, then further purified by Superose 6 size exclusion chromatography (GE Healthcare) in a buffer containing potassium phosphate 20mM pH8.0, NaCl 150mM, TCEP 1mM.

PRC2 complex (0.5 µg), dinucleosomes (0.5 µg), buffer (20 mM Tris-HCl pH8.0, 4 mM EDTA, 1mM PMSF and 0.5 mM DTT) and ^{3}H SAM (2 µl) in a total of 20 µl, were incubated for 1 h at 30°C and the reaction stopped by adding SDS-loading buffer. Samples were analysed by 18% SDS-PAGE, Coomassie stained, soaked in enhance solution and dried before exposing the gel to film overnight at -80°C.

PRC1 purification and ubiquitylation assay

PRC1 complex (Ring1B, Pcgf2, and Rybp) was coexpressed using baculovirus and purified from SF9 cells as previously described Tavares et al., 2012. GST-RPCD fusion protein (WT and mutants) were purified from bacteria using the same method as Ring1B Pcgf4 complex purification (Bentley et al., 2011). Briefly, the fusion protein was expressed in bacteria overnight grown at 16°C, and purified under native conditions using glutathione sepharose.

PRC1 ubiquitylation assays were performed using 10 µg/ml UBE1 E1 (Boston Biochem), 40 µg/ml UbcH5c E2 (Enzo life Sciences), 0.1 mg/ml methylated ubiquitin (R&D Systems), 0.2 mM ATP, 0.5µg dinucleosomes and 4 µg PRC1 or 4µg GST-RPCD fusion protein in a total volume of 20 µl. Assays were incubated for 1 h at 37°C and the reaction stopped by adding SDS-loading buffer. Samples were analysed by 18% SDS-PAGE and western blotting using H2AK119u1 and H3 antibodies.

Co-immunoprecipitation

ESCs were transfected as above and harvested 3 days after transfection. Cells were lysed in (20 mM HEPES pH 7.9, 1.5 mM MgCl2, 0.1 % NP40, 0.2 mM EDTA, 350 mM NaCl, 20 % glycerol, 0.5 mM DTT, and 1x cOmplete EDTA-free protease inhibitors) and incubated with Flag M2 agarose beads (Sigma). After extensive washing, bound proteins were eluted with FLAG peptide(100 µg/ml) and elutions were analysed by 12 % SDS-PAGE and western blot using the following antibodies : Flag (1:1000, Sigma M2 HRP conjugated), Ring1B (1:1000, (Atsuta et al., 2001), Rybp (1:500, Millipore, AB3637), Suz 12 (1:250, Cell signalling, 3737S).

Supplemental References

Anders, S., and Huber, W. (2010). Differential expression analysis for sequence count data. Genome biology *11*, R106.

Atsuta, T., Fujimura, S., Moriya, H., Vidal, M., Akasaka, T., and Koseki, H. (2001). Production of monoclonal antibodies against mammalian Ring1B proteins. Hybridoma *20*, 43-46.

Bentley, M.L., Corn, J.E., Dong, K.C., Phung, Q., Cheung, T.K., and Cochran, A.G. (2011). Recognition of UbcH5c and the nucleosome by the Bmi1/Ring1b ubiquitin ligase complex. The EMBO journal *30*, 3285-3297.

Blackledge, N.P., Zhou, J.C., Tolstorukov, M.Y., Farcas, A.M., Park, P.J., and Klose, R.J. (2010). CpG islands recruit a histone H3 lysine 36 demethylase. Molecular cell *38*, 179-190.

Flicek, P., Ahmed, I., Amode, M.R., Barrell, D., Beal, K., Brent, S., Carvalho-Silva, D., Clapham, P., Coates, G., Fairley, S*., et al.* (2013). Ensembl 2013. Nucleic acids research *41*, D48-55.

Lande-Diner, L., Zhang, J., Ben-Porath, I., Amariglio, N., Keshet, I., Hecht, M., Azuara, V., Fisher, A.G., Rechavi, G., and Cedar, H. (2007). Role of DNA methylation in stable gene repression. The Journal of biological chemistry *282*, 12194-12200.

Li, H., and Durbin, R. (2009). Fast and accurate short read alignment with Burrows-Wheeler transform. Bioinformatics *25*, 1754-1760.

Long, H.K., Sims, D., Heger, A., Blackledge, N.P., Kutter, C., Wright, M.L., Grutzner, F., Odom, D.T., Patient, R., Ponting, C.P*., et al.* (2013). Epigenetic conservation at gene regulatory elements revealed by non-methylated DNA profiling in seven vertebrates. eLife *2*, e00348.

Meyer, L.R., Zweig, A.S., Hinrichs, A.S., Karolchik, D., Kuhn, R.M., Wong, M., Sloan, C.A., Rosenbloom, K.R., Roe, G., Rhead, B*., et al.* (2013). The UCSC Genome Browser database: extensions and updates 2013. Nucleic acids research *41*, D64-69.

Peters, A.H., Kubicek, S., Mechtler, K., O'Sullivan, R.J., Derijck, A.A., Perez-Burgos, L., Kohlmaier, A., Opravil, S., Tachibana, M., Shinkai, Y*., et al.* (2003). Partitioning and plasticity of repressive histone methylation states in mammalian chromatin. Molecular cell *12*, 1577-1589.

Quinlan, A.R., and Hall, I.M. (2010). BEDTools: a flexible suite of utilities for comparing genomic features. Bioinformatics *26*, 841-842.

Schermelleh, L., Carlton, P.M., Haase, S., Shao, L., Winoto, L., Kner, P., Burke, B., Cardoso, M.C., Agard, D.A., Gustafsson, M.G*., et al.* (2008). Subdiffraction multicolor imaging of the nuclear periphery with 3D structured illumination microscopy. Science *320*, 1332-1336.

Sharif, J., Muto, M., Takebayashi, S., Suetake, I., Iwamatsu, A., Endo, T.A., Shinga, J., Mizutani-Koseki, Y., Toyoda, T., Okamura, K*., et al.* (2007). The SRA protein Np95 mediates epigenetic inheritance by recruiting Dnmt1 to methylated DNA. Nature *450*, 908-912.

Simon, M.D. (2010). Installation of site-specific methylation into histones using methyl lysine analogs. Current protocols in molecular biology / edited by Frederick M Ausubel [et al] *Chapter 21*, Unit 21 18 21-10.

Tavares, L., Dimitrova, E., Oxley, D., Webster, J., Poot, R., Demmers, J., Bezstarosti, K., Taylor, S., Ura, H., Koide, H*., et al.* (2012). RYBP-PRC1 complexes mediate H2A ubiquitylation at polycomb target sites independently of PRC2 and H3K27me3. Cell *148*, 664-678.

Tsumura, A., Hayakawa, T., Kumaki, Y., Takebayashi, S., Sakaue, M., Matsuoka, C., Shimotohno, K., Ishikawa, F., Li, E., Ueda, H.R*., et al.* (2006). Maintenance of self-renewal ability of mouse embryonic stem cells in the absence of DNA methyltransferases Dnmt1, Dnmt3a and Dnmt3b. Genes to cells : devoted to molecular & cellular mechanisms *11*, 805-814.

Zvetkova, I., Apedaile, A., Ramsahoye, B., Mermoud, J.E., Crompton, L.A., John, R., Feil, R., and Brockdorff, N. (2005). Global hypomethylation of the genome in XX embryonic stem cells. Nature genetics *37*, 1274-1279.